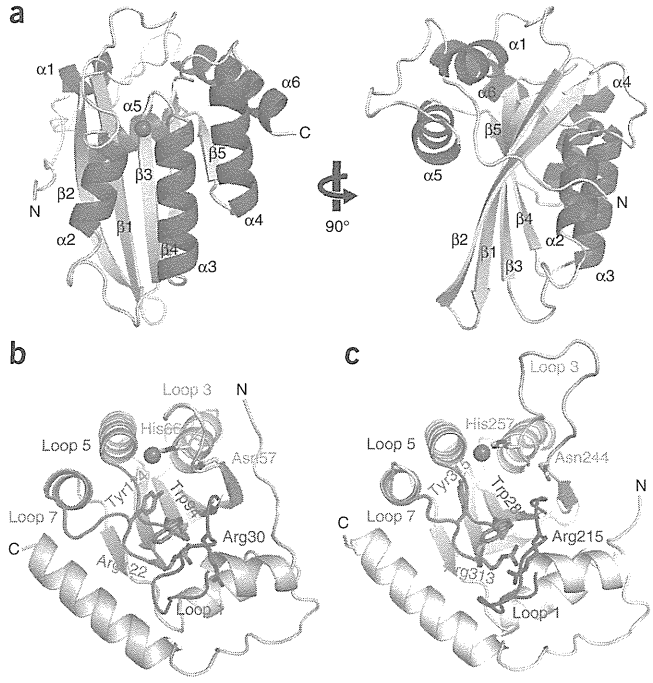

Figure 1 The X-ray crystal structure of full-length A3C. (**a**) Two views of the A3C structure, rotated by 90°, are shown. The α-helices (α1–α6) and β-strands (β1–β5) are colored in red and yellow, respectively. A coordinated zinc ion is represented as a blue sphere. (**b**,**c**) Structural comparison around the catalytic groove of A3C (**b**) and A3G CTD (**c**). Amino acid side chains of the conserved residues in loop 1 (magenta), loop 3 (yellow), loop 5 (orange) and loop 7 (cyan) are labeled with the residue numbers.

negatively charged residues. In addition, we found that the structural features of the Vif-binding interfaces are conserved in the homologous Z2-type A3C, A3F and A3DE proteins but not in the A3G protein. These results will deepen our understanding of A3-Vif interactions and aid in the development of new strategies using potential endogenous inhibitors against HIV-1.

RESULTS

High-resolution crystal structure of full-length A3C

Initially, human A3C was expressed in *Escherichia coli* as an N-terminal GST-tagged recombinant protein to increase its solubility. The tag was subsequently removed. We further purified the full-length A3C protein (residues 1–190) and solved its structure at 2.15 Å (**Fig. 1a** and **Table 1**). The A3C structure has a core platform composed of six α-helices (α1–α6) and five β-strands (β1–β5), with a coordinated zinc ion that is well conserved in the cytidine deaminase superfamily[22]. The superimposition of the A3C core onto that of the A3G CTD crystal structure (PDB 3IR2) for 86% of the backbone atoms exhibited a Cα r.m.s. deviation of 1.36 Å, thereby indicating the structural conservation of the core platform.

In contrast to the high conservation of the core structures, the loop regions, particularly loops 1, 3, 4 and 7 of the A3C and A3G CTD structures, are distinct (**Fig. 1b,c** and **Supplementary Fig. 1a,b**). Nevertheless, the positions of certain residues in the loops exhibit structural similarity. Arg30, Asn57, His66, Trp94, Arg122 and Tyr124 in A3C (**Fig. 1b**) are similar to Arg215, Asn244, His257, Trp285, Arg313 and Tyr315 in the A3G CTD (**Fig. 1c**). These residues primarily have critical roles in maintaining the conformation of the catalytic center and the groove involved in substrate binding[18,20], which are functionally conserved features among A3 proteins. In contrast, differences in the HIV-1 Vif interaction are attributable to unique conformational differences between the A3C and A3G CTD structures.

Notably, the A3C structure exhibits a continuous well-ordered β2-strand that is remarkably different from that of the A3G CTD (PDB 3IR2) (**Fig. 1** and **Supplementary Fig. 1a,b**). Molecular dynamics (MD) simulations support the high stability of the A3C β2 (**Supplementary Fig. 1c–f**), which is also observed in the APOBEC2 (A2) crystal structure[23]. In the A2 structure, a continuous β2 strand mediates dimerization through a β2 of another molecule. However, we did not detect any intermolecular contacts through the β2-β2 interaction within the 20 largest contacts in the crystal packing (**Supplementary Fig. 2a**). In addition, our dynamic light-scattering experiments indicated both monomodal and bimodal distributions of A3C proteins in solution (**Supplementary Fig. 2b**), although our gel-filtration data indicated that most of the protein was distributed in the monomer size fraction (**Supplementary Fig. 2c**). These results suggest that dynamic A3C dimerization might occur but not through their β2 strands. This effect might be partly owing to 13 amino acids of the N-terminal region, which reside on the β2 strand, that sterically hinder the β2-β2 associations. Recently, a similar observation with a full-length A2 structure has also been reported[24].

Ten A3C residues are critical for HIV-1 Vif binding

To determine the interface for HIV-1 Vif recognition of A3C, extensive structure-guided mutagenesis experiments were performed by using an approach analogous to that previously described for A3G[25]. A single

Table 1 Data collection and refinement statistics

	APOBEC3C
Data collection	
Space group	$P6_1$
Cell dimensions	
a, *b*, *c* (Å)	105.04, 105.04, 70.05
α, *β*, *γ* (°)	90, 90, 120
Resolution (Å)	105–2.15 (2.19–2.15)
R_{merge}	5.4 (33.8)
$I/\sigma I$	94.5 (13.3)
Completeness (%)	99.9 (100)
Redundancy	22.3 (22.6)
Refinement	
Resolution (Å)	91–2.15
No. reflections	22,783
R_{work} / R_{free}	21.4 / 26.3
No. atoms	3,281
Protein	3,188
Ligand/ion	3
Water	90
B factors	45.56
Protein	45.69
Ligand/ion	45.50
Water	40.90
R.m.s. deviations	
Bond lengths (Å)	0.012
Bond angles (°)	1.390

A single crystal was used for solving the structure. Values in parentheses are for highest-resolution shell.

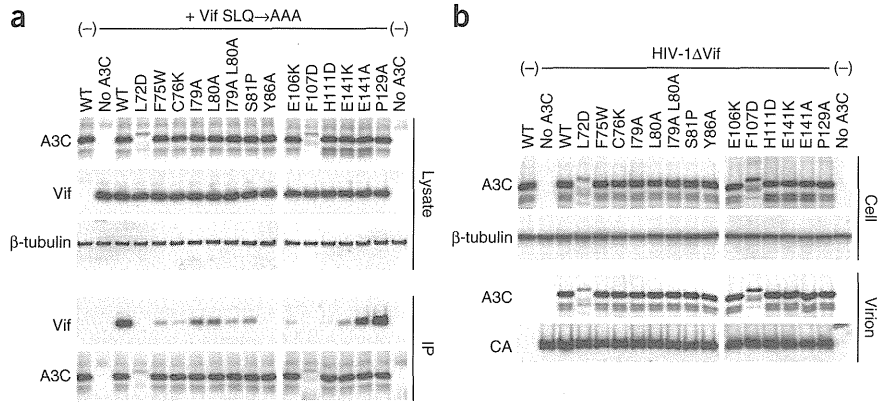

Figure 2 Ten A3C residues critical for HIV-1 Vif interaction. (**a**) Immunoblots of lysates and anti-His immunoprecipitates of HEK-293T cells with wild type (WT), mutant A3C-Myc-His or control plasmid (no A3C) expressed in the presence (+) or absence (–) of HIV-1 Vif SLQ→AAA. Immunoblotting is with anti-Vif or anti-His monoclonal antibodies as shown. Anti–β-tubulin antibody was used as a loading control. IP, immunoprecipitation. (**b**) Virion-packaging efficiency of Vif-resistant A3C mutants. Intracellular (cell) and virus-incorporated (virion) levels of A3C WT and mutants analyzed by western blotting. Samples are from cells transfected with HIV-1ΔVif or control plasmids (–), plus either A3C or control plasmids (no A3C). The HIV-1 capsid protein (CA) levels in virions were detected with an anti-p24 antibody.

E106K substitution changes the susceptibility of A3C to Vif-mediated degradation[10], which suggests that Glu106 is one of the residues responsible for the A3C-Vif interaction. Therefore, to further identify the other critical residues adjacent to Glu106, we first introduced substitution mutations near Glu106 and tested the Vif sensitivity *in vitro*. The results are summarized in **Supplementary Figure 3**. Wild-type A3C was not detectable when coexpressed with Vif (Vif sensitive), whereas the expression of the E106K mutant was unchanged in the presence of Vif (Vif resistant). These experiments were repeated for all residues whose mutations resulted in a Vif-resistant phenotype, until the surrounding A3C surface residues were all associated with sensitive mutants. The percentage reduction of A3C expression in the presence relative to the absence of Vif was evaluated (Vif-resistance level) (**Supplementary Fig. 3**). The results indicated that any single point mutation in the nine residues (Leu72, Phe75, Cys76, Ile79, Leu80, Ser81, Tyr86, Glu106 and Phe107) resulted in a >50% Vif-resistance level, whereas the mutations H111D and A109K resulted in 45% and 41% resistance, respectively. To evaluate whether these residues were intrinsically involved in the Vif interaction, we immunoprecipitated a Vif SOCS-box mutant (Vif SLQ→AAA) that can bind A3 but not EloBC[8,26,27] in the presence of wild-type or Myc-His-tagged A3C mutants, and immunoblotted for Vif SLQ→AAA (**Fig. 2a**). Vif was coimmunoprecipitated with wild-type A3C and A3C P129A at equal levels (**Fig. 2a**), which indicated that Pro129 in A3C is not responsible for the Vif interaction, unlike findings with A3G[16]. In contrast, all of the Vif-resistant A3C mutants immunoprecipitated minimal amounts of Vif, which indicated that the residues whose mutations conferred the Vif-resistant phenotypes are indeed critical for the Vif interaction. The E141K mutation abolished Vif binding, despite being relatively Vif sensitive. The reason for this effect is not clear. These findings demonstrated that Leu72, Phe75, Cys76, Ile79, Leu80, Ser81, Tyr86, Glu106, Phe107 and His111 are involved in forming the Vif-interaction interface. All of the binding-deficient A3C mutants were incorporated into *vif*-deficient HIV-1 (HIV-1ΔVif) as efficiently as wild-type A3C (**Fig. 2b**), which suggested that RNA-binding capacity was not impaired by the A3C mutations.

Structural mapping of the mutagenesis results yielded a Vif-resistance level, which is color-coded on the structure (**Fig. 3a,b**). The residues involved in the Vif interaction are located in an area between the α2 and α3 helices, distal from the Pro129 of the A3G DPD motif[16]. Notably, in the A3C surface representation, the interface is a shallow cavity composed of hydrophobic (Leu72, Ile79 and Leu80) or aromatic (Phe75, Tyr86, Phe107 and His111) residues at the bottom and hydrophilic (Cys76, Ser81 and Glu106) residues at the edges (**Fig. 3a–c**). One notable feature of this cavity is that two potential π interactions can be observed at the bottom, on the basis of the configuration of four aromatic residues (Phe75, Tyr86, Phe107

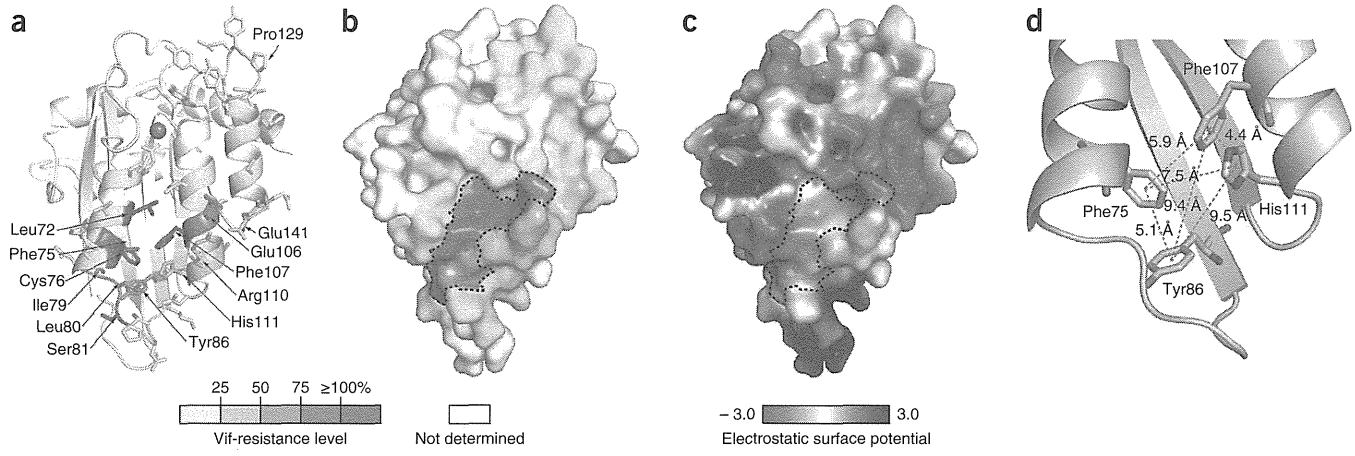

Figure 3 The A3C interface for the HIV-1 Vif interaction. (**a**,**b**) The A3C structure, displaying critical residues for Vif sensitivity. The residues are colored in the ribbon (**a**) and surface (**b**) representations of A3C according to the resistance level of Vif-mediated degradation, as shown in the bottom bar. Residues exhibiting a >50% Vif-resistance level are enclosed by a dotted line. (**c**) The electrostatic potential of A3C is shown. The accessible surface area is colored according to the calculated electrostatic potential from –3 *kT/e* (red) to 3 *kT/e* (blue). The orientation and the dotted line are the same as in **b**. (**d**) Potential π-stacking interactions at the Vif-binding interface in A3C. The distances between the four aromatic residues involved in the Vif-binding cavity (Phe75, Tyr86, Phe107 and His111) are shown.

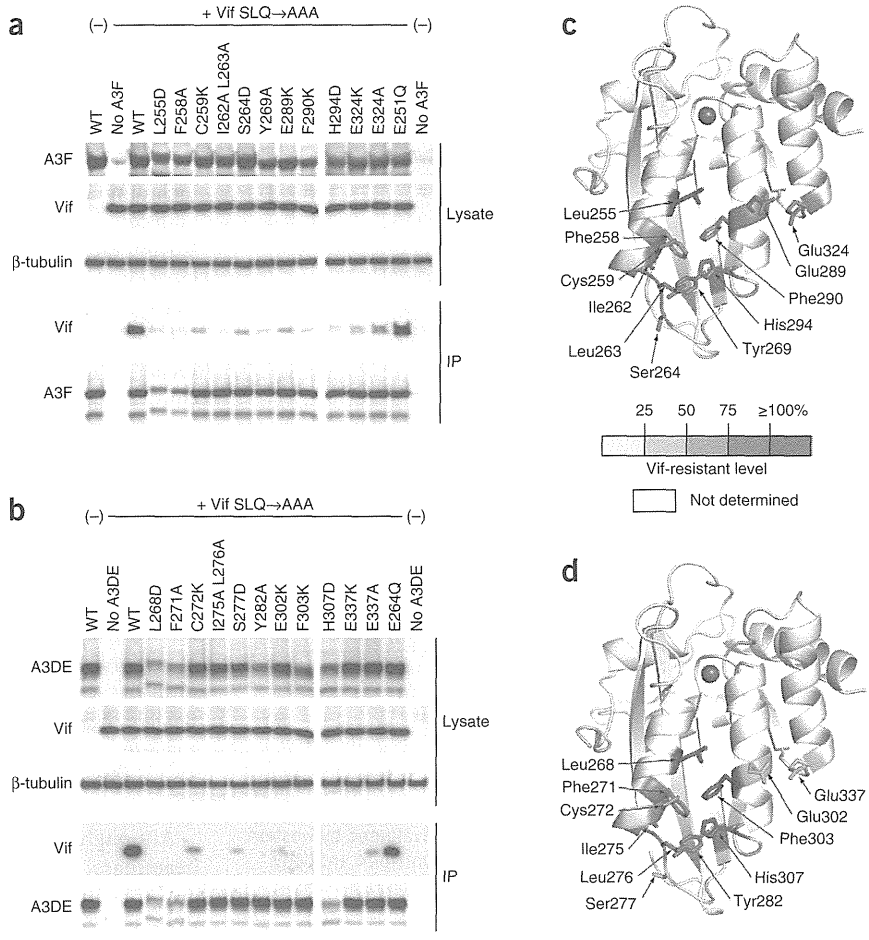

Figure 4 Analogous residues of A3F and A3DE are involved in the HIV-1 Vif-binding interface. (**a**,**b**) Coimmunoprecipitation (IP) of HIV-1 Vif SLQ→AAA with wild type (WT) or A3F-MycHIS mutants (**a**) and with wild type or A3DE-MycHIS mutants (**b**). (**c**,**d**) Residues are mapped on the A3F (**c**) or the A3DE CTD (**d**) structures modeled on the A3C crystal structure. The residues are color coded according to their Vif-resistance levels. A coordinated zinc ion is shown as a blue sphere.

and His111) (**Fig. 3d**). Both Phe75-Tyr86 and Phe107-His111 show the proper distance and orientation to make two weak π-π interactions. In contrast, the pair of Phe75-Phe107 shows theoretically proper distance, although the angle is not appropriate to form a potential interaction. In addition, because a mutation of the hydrophobic or aromatic residues disrupts the Vif interaction and subsequent degradation, a specific size of the hydrophobic side chains, as well as π stacking, may be important for maintaining the correct interface conformation and for the A3C-Vif interaction. The interface includes a flexible region, loop 4, where Cys76, Ile79, Leu80 and Ser81 exhibit higher temperature factors in the crystal-structure data and in the MD simulations (**Supplementary Fig. 1f**), which suggests a partially flexible interface. Furthermore, the electrostatic surface potential analysis revealed a negatively charged interface (**Fig. 3c**), and substitutions with positively charged residues increase the Vif-resistance levels (**Supplementary Fig. 3**), which suggests that the negative electrostatic surface at the interface is also an important feature for HIV-1 Vif binding.

Vif-binding interfaces are conserved in A3C, A3F and A3DE

We also performed analogous coimmunoprecipitation experiments with equivalent mutations in the A3F and A3DE CTDs and tested for Vif interaction (**Fig. 4**). For A3F, involvement of the A3F Glu289 and Glu324 residues in Vif interaction has been reported[10,17]. Coimmunoprecipitates of these A3F mutants contained significantly reduced amounts of Vif (**Fig. 4a**) compared to wild type or E251Q (a mutation at the catalytic center), which demonstrates that the equivalent residues of A3F, Leu255, Phe258, Cys259, Ile262, Leu263, Ser264, Tyr269, Glu289, Phe290 and His294, are also important for the Vif interaction. In addition, we assessed the Vif sensitivity of the mutants (**Supplementary Fig. 3c**,**e**) and mapped the residues onto a homology model of the A3F CTD (**Fig. 4c**). Again, these residues were clustered and formed a Vif-binding cavity homologous to that observed in the A3C structure, although a slight difference in the Vif-resistant phenotype was observed. The E141K A3C mutant displayed a low Vif-resistance level (27%), whereas the corresponding A3F mutant, E324K, had a high resistance level (87%) (**Supplementary Fig. 3c**,**e**). MD simulations suggested that conformational differences at the negatively charged edge of the cavity may be responsible for these differences (**Supplementary Fig. 4**).

For A3DE, the analysis of the coimmunoprecipitation assays demonstrated that 10 equivalent residues (Leu268, Phe271, Cys272, Ile275, Leu276, Ser277, Tyr282, Glu302, Phe303 and His307) of A3DE are also important for Vif interaction (**Fig. 4b**). In addition, mutations at any of the residues critical for Vif interaction resulted in a Vif-resistant phenotype, although the A3DE S277D and E302K mutants presented a lower of the Vif-resistance than the equivalents of A3F S264D and E289K, respectively (**Supplementary Fig. 3c–f**). Moreover, these residues provide a similar Vif-binding interface to that of A3C (**Fig. 4d**). These results suggest that the conformation of the Vif-interaction interface is highly conserved among A3C and the CTDs of A3F and A3DE.

To further assess whether the Z2-type A3G NTD provides a similar Vif-interaction interface at the equivalent position between the α2 and α3 helices, we constructed four analogous A3G mutants, F74W, L80D, Y86A and F107K, that have a substitution at identical residues, on the basis of sequence alignments between A3C and the A3G NTD. Examination of Vif sensitivity in these mutants indicated that none of these mutations in the A3G NTD changed the Vif-sensitive phenotype (**Supplementary Fig. 5**). These results demonstrated that the Vif-binding interface of A3G NTD is distinct from that of A3C, A3F and A3DE. In addition, they suggest that mutations between the α2 and α3 helices do not distort the presumed Vif-binding interface conformation of the A3G NTD.

Vif-resistant A3F inhibits HIV-1 infection

To elucidate the effects of the A3F mutations on viral incorporation, we analyzed the amounts of wild-type and mutant A3F proteins in cells and virions. Both wild-type and mutant A3F were efficiently incorporated into virus particles, with the exception of the H294D

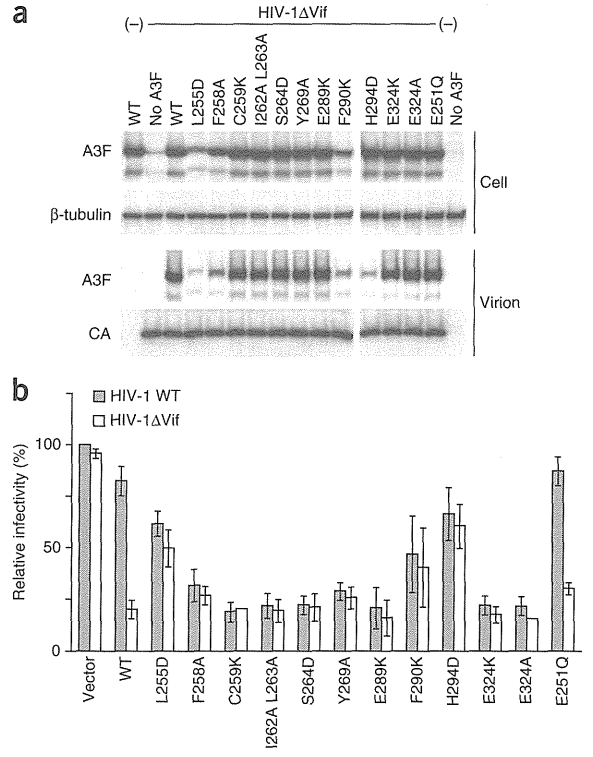

Figure 5 The effects of mutations at the equivalent residues in A3F on antiviral activity. (**a**) Intracellular expression (cell) and incorporation of wild-type A3F and the mutants into virions (virion), evaluated by western blotting. The CA level in virions was detected by an anti-p24 antibody. (**b**) The antiviral effects of A3F and mutants on wild-type HIV-1 (HIV-1 WT) or HIV-1ΔVif in a single-round replication assay with LuSIV cells. The relative viral infectivity of wild-type HIV-1 in the absence of A3F (vector) was set to 100%. Relative infectivity data are shown as means ± s.d. of three independent experiments.

mutant (**Fig. 5a**). This result suggests that the critical residues for Vif interaction (except for His294) of A3F are not located in the region that is responsible for A3F packaging into virions. Finally, to evaluate whether the A3F mutants exhibited any antiviral activity against HIV-1, we compared the infectivity of wild-type HIV-1 and HIV-1ΔVif in the presence of wild-type or mutant A3F. The wild-type A3F and the E251Q mutant reduced HIV-1ΔVif infectivity to 21% and 30%, respectively, whereas wild-type HIV-1 infectivity was only marginally affected (**Fig. 5b**). In contrast, all of the Vif-resistant A3F mutants suppressed the infectivity of wild-type HIV-1 as efficiently as for HIV-1ΔVif, which is consistent with their packaging level (**Fig. 5a,b**). These findings demonstrate that a disruption of the A3F-Vif interaction prevents A3F degradation and thereby allows A3F to be efficiently packaged into HIV-1 virions to exert its antiviral activity.

DISCUSSION

Studies conducted over the past decade have established that HIV-1 Vif abolishes the antiviral activity of A3 by recruiting an E3 ubiquitin ligase complex to promote proteasomal degradation. Many efforts toward developing strategies that interfere with the A3-Vif interaction have been unsuccessful to date, in part because of the lack of available structural information on the A3-Vif interaction interface. Here, we present, to our knowledge, the first crystal structure of A3C containing an HIV-1 Vif-interaction interface. In addition, our extensive structure-guided mutagenesis revealed the precise Vif-interaction site, between the α2 and α3 helices of A3C, and permitted the delineation of structural features (negatively charged, hydrophobic and partially flexible) in the Vif-interaction interface. Additional investigations demonstrated that the Vif-binding interfaces are highly conserved among Z2-type cytidine deaminases, including A3C, A3F and A3DE, but not A3G.

In combination with the A3C structure, our results suggest that the Vif-interaction interface forms a shallow cavity that is composed of hydrophobic and negatively charged residues. Notably, the positively charged DRMR motif (residues 14–17)[26] and hydrophobic residues (Leu24, Val25, Leu64, Ile66 and Leu72) on HIV-1 Vif are required for its specific interaction with A3C (reviewed in ref. 28), thereby confirming that both the electrostatic and hydrophobic interactions are the fundamental driving force for the A3C-Vif interaction. In addition, Vif Trp5, Trp21, Trp38, Tyr69, Trp70 and Trp89 are commonly considered essential for the interaction with A3C, A3F, A3DE or A3G. These data suggest that the π interactions of the aromatic residues between the A3C interface and Vif may contribute to their association, and these interactions are presumably common to all A3-Vif interactions. Recent reports indicate that Vif Trp21 and Trp38 are important for binding with the cofactor CBF-β. The π interactions may be mediated by CBF-β for efficient formation of the E3 ubiquitin ligase complex[4,5,29]. In addition, the existence of a partially flexible region in the Vif-binding interface (**Supplementary Fig. 1f**) suggests that the cavity may not locally exhibit a fixed conformation, and certain structural changes may be induced by Vif to allow a tight interaction.

Although the A3G NTD is categorized as a Z2-type cytidine deaminase, the amino acid sequences of the A3G NTD and A3C are quite different; only 42.8% of the A3C sequences are identical to the A3G NTD, whereas 77% and 76% are identical to the A3F CTD and A3DE CTD sequences, respectively. In particular, the residues of the α2–α3 regions are not homologous between A3C, A3F, A3DE and the A3G NTD, which suggests differences in their local conformations. For A3C, the Vif-binding interface is located in a region distal to loop 7 that corresponds to an area of the DPD motif in the A3G NTD. In addition, our homologous mutagenesis showed that the equivalent area of the A3G NTD between the α2 and α3 helices is not critical for the A3G-Vif interaction (**Supplementary Fig. 5**), demonstrating that two different regions in A3C and the A3G NTD molecules participate in each specific interaction with Vif. The presence of these distinct interfaces is consistent with the evidence that the HIV-1 Vif residues responsible for binding to A3 proteins are different. The YRHHY motif (residues 40–44) and the DRMR motif in Vif are involved in specific interactions with A3G, and A3C, A3F or A3DE, respectively[11,26,30–33]. Nevertheless, because both types of A3-Vif interactions fundamentally require electrostatic and hydrophobic bindings and the involvement of the flexible loop conformations (loop 4 for A3C, A3F or A3DE; loop 7 for A3G), the interfaces of A3C, A3F or A3DE and A3G may have similar structural characteristics.

Our determination of the high-resolution A3C crystal structure and extensive structure-guided mutagenesis revealed the A3C structural features associated with the Vif interaction. In addition, the conformation of the Vif-binding interface is highly conserved within the Z2-type A3 subfamily. The location of the Vif-binding interface on A3 proteins may prove to be important during the development of pharmacologic agents that target A3-Vif interactions. Previous reports have shown that the residues of A3G and A3C that are critical for nucleic acid binding also have essential roles in the efficient packaging

of A3 into virions[16,34]. These residues are involved in the formation of nucleic acid–binding grooves primarily consisting of loops 1, 3, 5 and 7 near the coordinated zinc ions of A3G and A3C proteins. The A3G DPD motif for Vif interaction is immediately adjacent to the four YYFW residues (124–127) necessary for A3G incorporation into virions[16]. Therefore, we must use caution to not perturb the contributions of the neighboring YYFW residues that are necessary for A3G incorporation into virions. In contrast, the Vif-binding interfaces that we identified in A3C, A3F and A3DE are mapped to a position distal to the nucleic acid–binding pocket that is important for A3's encapsidation into virions. Therefore, during drug discovery and development, it could be advantageous to target the interaction of Vif with A3C, A3F or A3DE, particularly that with A3F, without disturbing the nucleic acid–binding capability. Taken together, these findings on the structural features of Vif-binding interfaces may aid in our understanding of Vif-A3 interactions and lead to the development of new pharmacologic anti-HIV-1 compounds that could restore the activity of the intrinsic antiviral factor in the context of HIV-1 infection.

METHODS

Methods and any associated references are available in the online version of the paper.

Accession codes. Coordinates and structure factors have been deposited into the Protein Data Bank, with the accession code 3VOW.

Note: Supplementary information is available in the online version of the paper.

ACKNOWLEDGMENTS

We thank A.M. Gronenborn, J.G. Levin and K. Strebel for critical discussions and reading of the manuscript. We also thank K. Tokunaga (National Institute of Infectious Diseases, Tokyo, Japan) for providing the pCAGGS APOBEC3 plasmids. This work was supported in part by a grant from the Ministry of Education, Culture, Sports, Science and Technology of Japan to Y.I. (JSPS KAKENHI 24590568) and by a grant for HIV/AIDS research from the Ministry of Health, Labor and Welfare of Japan to Y.I.

AUTHOR CONTRIBUTIONS

S.K., H.O., M.N., T.K., T.Y., N.W., A.S. and Y.I. performed experiments and analysis for the crystal structure determination; S.K., M.N., M.I., Y.N., T.K., Y.Y. and Y.I. performed biochemical experiments; S.K., M.N., M.I., Y.N., Y.Y., W.S. and Y.I. analyzed the biochemical data; Y.I. directed the project; S.K., H.O. and Y.I. wrote the manuscript with all authors' help.

COMPETING FINANCIAL INTERESTS

The authors declare no competing financial interests.

Published online at http://www.nature.com/doifinder/10.1038/nsmb.2378.
Reprints and permissions information is available online at http://www.nature.com/reprints/index.html.

1. Goila-Gaur, R. & Strebel, K. HIV-1 Vif, APOBEC, and intrinsic immunity. *Retrovirology* **5**, 51 (2008).
2. LaRue, R.S. *et al.* Guidelines for naming nonprimate APOBEC3 genes and proteins. *J. Virol.* **83**, 494–497 (2009).
3. Wedekind, J.E., Dance, G.S., Sowden, M.P. & Smith, H.C. Messenger RNA editing in mammals: new members of the APOBEC family seeking roles in the family business. *Trends Genet.* **19**, 207–216 (2003).
4. Jäger, S. *et al.* Vif hijacks CBF-β to degrade APOBEC3G and promote HIV-1 infection. *Nature* **481**, 371–375 (2012).
5. Zhang, W., Du, J., Evans, S.L., Yu, Y. & Yu, X.F. T-cell differentiation factor CBF-β regulates HIV-1 Vif-mediated evasion of host restriction. *Nature* **481**, 376–379 (2012).
6. Marin, M., Rose, K.M., Kozak, S.L. & Kabat, D. HIV-1 Vif protein binds the editing enzyme APOBEC3G and induces its degradation. *Nat. Med.* **9**, 1398–1403 (2003).
7. Sheehy, A.M., Gaddis, N.C. & Malim, M.H. The antiretroviral enzyme APOBEC3G is degraded by the proteasome in response to HIV-1 Vif. *Nat. Med.* **9**, 1404–1407 (2003).
8. Yu, X. *et al.* Induction of APOBEC3G ubiquitination and degradation by an HIV-1 Vif-Cul5-SCF complex. *Science* **302**, 1056–1060 (2003).
9. Russell, R.A., Smith, J., Barr, R., Bhattacharyya, D. & Pathak, V.K. Distinct domains within APOBEC3G and APOBEC3F interact with separate regions of human immunodeficiency virus type 1 Vif. *J. Virol.* **83**, 1992–2003 (2009).
10. Smith, J.L. & Pathak, V.K. Identification of specific determinants of human APOBEC3F, APOBEC3C, and APOBEC3DE and African green monkey APOBEC3F that interact with HIV-1 Vif. *J. Virol.* **84**, 12599–12608 (2010).
11. Zhen, A., Wang, T., Zhao, K., Xiong, Y. & Yu, X.F. A single amino acid difference in human APOBEC3H variants determines HIV-1 Vif sensitivity. *J. Virol.* **84**, 1902–1911 (2010).
12. Bogerd, H.P., Doehle, B.P., Wiegand, H.L. & Cullen, B.R. A single amino acid difference in the host APOBEC3G protein controls the primate species specificity of HIV type 1 virion infectivity factor. *Proc. Natl. Acad. Sci. USA* **101**, 3770–3774 (2004).
13. Mangeat, B., Turelli, P., Liao, S. & Trono, D. A single amino acid determinant governs the species-specific sensitivity of APOBEC3G to Vif action. *J. Biol. Chem.* **279**, 14481–14483 (2004).
14. Schröfelbauer, B., Chen, D. & Landau, N.R. A single amino acid of APOBEC3G controls its species-specific interaction with virion infectivity factor (Vif). *Proc. Natl. Acad. Sci. USA* **101**, 3927–3932 (2004).
15. Xu, H. *et al.* A single amino acid substitution in human APOBEC3G antiretroviral enzyme confers resistance to HIV-1 virion infectivity factor-induced depletion. *Proc. Natl. Acad. Sci. USA* **101**, 5652–5657 (2004).
16. Huthoff, H. & Malim, M.H. Identification of amino acid residues in APOBEC3G required for regulation by human immunodeficiency virus type 1 Vif and Virion encapsidation. *J. Virol.* **81**, 3807–3815 (2007).
17. Albin, J.S. *et al.* A single amino acid in human APOBEC3F alters susceptibility to HIV-1 Vif. *J. Biol. Chem.* **285**, 40785–40792 (2010).
18. Chen, K.M. *et al.* Structure of the DNA deaminase domain of the HIV-1 restriction factor APOBEC3G. *Nature* **452**, 116–119 (2008).
19. Furukawa, A. *et al.* Structure, interaction and real-time monitoring of the enzymatic reaction of wild-type APOBEC3G. *EMBO J.* **28**, 440–451 (2009).
20. Holden, L.G. *et al.* Crystal structure of the anti-viral APOBEC3G catalytic domain and functional implications. *Nature* **456**, 121–124 (2008).
21. Shandilya, S.M. *et al.* Crystal structure of the APOBEC3G catalytic domain reveals potential oligomerization interfaces. *Structure* **18**, 28–38 (2010).
22. Betts, L., Xiang, S., Short, S.A., Wolfenden, R. & Carter, C.W.J. Cytidine deaminase. The 2.3 Å crystal structure of an enzyme: transition-state analog complex. *J. Mol. Biol.* **235**, 635–656 (1994).
23. Prochnow, C., Bransteitter, R., Klein, M.G., Goodman, M.F. & Chen, X.S. The APOBEC-2 crystal structure and functional implications for the deaminase AID. *Nature* **445**, 447–451 (2007).
24. Krzysiak, T.C., Jung, J., Thompson, J., Baker, D. & Gronenborn, A.M. APOBEC2 is a monomer in solution: implications for APOBEC3G models. *Biochemistry* **51**, 2008–2017 (2012).
25. Iwatani, Y. *et al.* HIV-1 Vif-mediated ubiquitination/degradation of APOBEC3G involves four critical lysine residues in its C-terminal domain. *Proc. Natl. Acad. Sci. USA* **106**, 19539–19544 (2009).
26. Russell, R.A. & Pathak, V.K. Identification of two distinct human immunodeficiency virus type 1 Vif determinants critical for interactions with human APOBEC3G and APOBEC3F. *J. Virol.* **81**, 8201–8210 (2007).
27. Larue, R.S., Lengyel, J., Jónsson, S.R., Andrésdóttir, V. & Harris, R.S. Lentiviral Vif degrades the APOBEC3Z3/APOBEC3H protein of its mammalian host and is capable of cross-species activity. *J. Virol.* **84**, 8193–8201 (2010).
28. Kitamura, S., Ode, H. & Iwatani, Y. Structural features of antiviral APOBEC3 proteins are linked to their functional activities. *Front. Microbiol.* **2**, 258 (2011).
29. Hultquist, J.F., Binka, M., Larue, R.S., Simon, V. & Harris, R.S. Vif proteins of human and simian immunodeficiency viruses require cellular CBFβ to degrade APOBEC3 restriction factors. *J. Virol.* **86**, 2874–2877 (2012).
30. He, Z., Zhang, W., Chen, G., Xu, R. & Yu, X.F. Characterization of conserved motifs in HIV-1 Vif required for APOBEC3G and APOBEC3F interaction. *J. Mol. Biol.* **381**, 1000–1011 (2008).
31. Pery, E., Rajendran, K.S., Brazier, A.J. & Gabuzda, D. Regulation of APOBEC3 proteins by a novel YXXL motif in human immunodeficiency virus type 1 Vif and simian immunodeficiency virus SIVagm Vif. *J. Virol.* **83**, 2374–2381 (2009).
32. Schröfelbauer, B., Senger, T., Manning, G. & Landau, N.R. Mutational alteration of human immunodeficiency virus type 1 Vif allows for functional interaction with nonhuman primate APOBEC3G. *J. Virol.* **80**, 5984–5991 (2006).
33. Tian, C. *et al.* Differential requirement for conserved tryptophans in human immunodeficiency virus type 1 Vif for the selective suppression of APOBEC3G and APOBEC3F. *J. Virol.* **80**, 3112–3115 (2006).
34. Stauch, B. *et al.* Model structure of APOBEC3C reveals a binding pocket modulating ribonucleic acid interaction required for encapsidation. *Proc. Natl. Acad. Sci. USA* **106**, 12079–12084 (2009).

ONLINE METHODS

Plasmids and antibodies. To construct a plasmid to express A3C in bacteria, a DNA fragment (573 base pairs) was inserted into pET41a(+) (Novagen), which has an N-terminal GST tag and an enterokinase cleavage site. This construct was designated pET41 GST-A3C. A3 expression plasmids for mammalian cells were constructed by replacing the A3G gene of pcDNA A3G (Myc-His)[35] with the cDNA fragments of the A3 derived from pCAGGS APOBEC3 (ref. 36). Substitutions of the A3 residues were introduced into the A3 expression plasmids as previously described[25]. pcDNA-HVif SLQ→AAA was generated by site-directed mutagenesis from pcDNA-HVif[37]. For all mutants, the sequences of both the insert and the boundary regions were verified by DNA sequencing. The pNL4-3 WT and pNL4-3*vif*(−) plasmids were described previously[25]. Anti-p24 (CA) rabbit serum (4250) and a peptide antibody (C-17 rabbit serum; 10082) for human A3G were obtained from the AIDS Research and Reference Reagent Program, National Institute of Allergy and Infectious Diseases, US National Institutes of Health, Germantown, Maryland, USA. Anti-His mAb (D291-3) and anti-His rabbit serum (PM032) (Medical & Biological Laboratories Co.) and anti-Vif mAb (ab66643) and anti–β-tubulin rabbit polyclonal antibody (ab6046; Abcam) were purchased.

Protein expression and purification. Rosetta2(DE3)pLysS bacterial cells (Novagen) transformed with pET41 GST-A3C, were grown at 37 °C in Luria-Bertani medium containing 25 μg ml^{-1} of kanamycin and 34 μg ml^{-1} of chloramphenicol until reaching an optical density at 600 nm (OD_{600}) of 0.6. After the addition of 1 mM IPTG and 1 μM $ZnSO_4$, the cells were further incubated to express the GST-A3C at 20 °C for 20 h. The bacterial pellets were collected by centrifugation and resuspended with a lysis buffer (1,000 mM NaCl, 10 mM $CaCl_2$, 1 mM EDTA, 10% glycerol, 5 mM 2-mercaptoethanol (2-ME) and 25 mM HEPES, pH 7.0). The lysed cells were disrupted by sonication and French press and then subjected to centrifugation and filtration. The supernatant was applied to a glutathione Sepharose 4 FF column (GE Healthcare) for affinity purification. The bound GST-A3C was eluted by an elution buffer (500 mM NaCl, 10 mM $CaCl_2$, 10% glycerol, 5 mM 2-ME, 40 mM reduced L-glutathione and 50 mM Tris HCl, pH 8.0). The eluate was digested by recombinant enterokinase (Novagen) in a cleavage buffer (350 mM NaCl, 12 mM $CaCl_2$, 2% glycerol, 1 mM 2-ME, 1% Triton X-100 and 30 mM Tris HCl, pH 7.4) at 20 °C overnight. The digested A3C was purified by using SPXL cation-exchange chromatography (GE Healthcare) with IEX start buffer (10% glycerol, 5 mM 2-ME and 50 mM Tris HCl, pH 8.0) and IEX elution buffer (IEX start buffer containing 1,000 mM NaCl and 200 mM L-arginine hydrochloride (L-Arg HCl)). A3C was further purified by using Superdex-75 gel filtration chromatography (GE Healthcare).

Protein crystallization. The A3C was dialyzed with crystallization buffer (50 mM NaCl, 300 mM L-Arg HCl, 1 mM Tris(2-carboxyethyl)phosphine hydrochloride (TCEP) and 10 mM HEPES, pH 8.0) and then concentrated to approximately 10 mg ml^{-1} by using Amicon Ultra-0.5 ml (Millipore). The initial crystallization screening was performed at 20 °C by using a JCSG-*plus* Screen solution (Molecular Dimensions) containing 300 mM L-Arg HCl by the hanging-drop vapor-diffusion method. A crystal formed in a condition containing 85 mM bicine (pH 9.0), 17% PEG6000 and 300 mM L-Arg HCl. A better-shaped crystal was grown at 20 °C with 300 μl of reservoir solution (14% PEG6000, 300 mM L-Arg HCl and 85 mM bicine, pH 9.0) by the hanging-drop vapor-diffusion method.

Data collection and processing. The crystal was soaked in a cryoprotectant solution (30% PEG6000, 300 mM L-Arg HCl and 85 mM bicine, pH 9.0) for a few seconds and flash cooled in nitrogen gas. Diffraction data sets were collected at 95 K by using synchrotron radiation (λ = 0.98 Å) on beamline BL-17A at the Photon Factory, KEK (Tsukuba, Japan). The data sets were indexed, integrated and scaled using the HKL2000 program package[38].

Analysis of structure data and construction of structure models. The structure was determined by the molecular replacement method, starting with the A3G 191–384-2K3A crystal structure (PDB 3IR2)[21] by using the program MolRep[39] and was manually built with the program COOT[40]. The structure refinement was performed by using REFMAC5 (ref. 41). The refinement statistics data are summarized in **Table 1**. Structure models of the A3F and DE CTDs were constructed on the basis of our A3C crystal structure by using Discovery Studio 3.0 (Accelrys).

Assays for Vif-dependent degradation of A3. A3C, A3F, A3DE or the mutant A3 expression plasmids (2 μg) and pcDNA-HVif or pcDNA 3.1 (−) control (that is, empty) vector (4 μg) were cotransfected into human embryonic kidney cells (293T) in 6-well plates by using FuGENE HD (Roche). At 48 h after transfection, cell lysates were prepared with Laemmli buffer (Bio-Rad) containing 2.5% 2-ME. Cell lysates were subjected to SDS-PAGE, and the proteins were transferred to Immobilon-P membranes (Millipore). The membranes were first incubated with appropriate antibodies as specified and were then incubated with horseradish peroxidase–conjugated secondary antibodies (Pierce). Protein bands were visualized by enhanced chemiluminescence by using SuperSignal West Dura (Pierce) and analyzed using ImageQuant TL (GE Healthcare).

Coimmunoprecipitation assays. To assess the Vif-A3 interaction *in vivo*, a coimmunoprecipitation assay was performed. Briefly, 293T cells were cotransfected with an A3 plasmid containing a lysine-free Myc-His tag and with pcDNA-HVif SLQ→AAA. At 48 h after transfection, the cells were harvested and then lysed in lysis buffer (150 mM NaCl, 1 mM EDTA, 1% Triton X-100, 10 μg ml^{-1} of RNase A in PBS) plus a protease-inhibitor cocktail (Sigma). Protein complexes were immunoprecipitated with anti-His rabbit serum and Protein G-Dynabeads (Invitrogen) at 4 °C. The beads were washed with lysis buffer and then analyzed with anti-His mAb and anti-Vif mAb for A3 protein and Vif, respectively.

Infectivity assays with LuSIV cells. Virus production and analysis of virus infectivity were performed as reported previously[25]. Briefly, to obtain virus particles, HeLa cells were cotransfected with 4 μg of pNL4-3 WT or pNL4-3*vif*(−) plus 2 μg of pcDNA-A3 or pcDNA 3.1 (−) (vector control). Virus infectivity was determined by single-cycle replication assays with LuSIV cells[42], obtained from the AIDS Research and Reference Reagent Program, National Institute of Allergy and Infectious Diseases, US National Institutes of Health, Germantown, Maryland, USA (originally from J.W. Roos and J.E. Clements). Infectivity was calculated by normalizing for the amount of input CA, determined by p24 antigen ELISA (ZeptoMetrix).

Incorporation of A3 proteins into virions. A3 incorporation was analyzed as previously described[25].

35. Kao, S. *et al.* The human immunodeficiency virus type 1 Vif protein reduces intracellular expression and inhibits packaging of APOBEC3G (CEM15), a cellular inhibitor of virus infectivity. *J. Virol.* **77**, 11398–11407 (2003).
36. Kinomoto, M. *et al.* All APOBEC3 family proteins differentially inhibit LINE-1 retrotransposition. *Nucleic Acids Res.* **35**, 2955–2964 (2007).
37. Nguyen, K.L. *et al.* Codon optimization of the HIV-1 *vpu* and *vif* genes stabilizes their mRNA and allows for highly efficient Rev-independent expression. *Virology* **319**, 163–175 (2004).
38. Otwinowski, Z. & Minor, W. Processing of X-Ray diffraction data collected in oscillation mode. *Methods Enzymol.* **276**, 307–326 (1997).
39. Vargin, A. & Teplyakov, A. MOLREP: an automated program for molecular replacement. *J. Appl. Crystallogr.* **30**, 1022–1025 (1997).
40. Emsley, P., Lohkamp, B., Scott, W.G. & Cowtan, K. Features and development of Coot. *Acta Crystallogr. D Biol. Crystallogr.* **66**, 486–501 (2010).
41. Murshudov, G.N., Vagin, A.A. & Dodson, E.J. Refinement of macromolecular structures by the maximum-likelihood method. *Acta Crystallogr. D Biol. Crystallogr.* **53**, 240–255 (1997).
42. Roos, J.W., Maughan, M.F., Liao, Z., Hildreth, J.E. & Clements, J.E. LuSIV cells: a reporter cell line for the detection and quantitation of a single cycle of HIV and SIV replication. *Virology* **273**, 307–315 (2000).

OPEN ACCESS Freely available online

PLOS ONE

The Carboxyl-Terminus of Human Immunodeficiency Virus Type 2 Circulating Recombinant form 01_AB Capsid Protein Affects Sensitivity to Human TRIM5α

Tadashi Miyamoto[1], Emi E. Nakayama[1], Masaru Yokoyama[2], Shiro Ibe[3], Shunpei Takehara[1], Ken Kono[1], Yoshiyuki Yokomaku[3], Massimo Pizzato[4], Jeremy Luban[4], Wataru Sugiura[3], Hironori Sato[2], Tatsuo Shioda[1]*

1 Department of Viral Infections, Research Institute for Microbial Diseases, Osaka University, Suita Osaka, Japan, **2** Laboratory of Viral Genomics, Pathogen Genomics Center, National Institute of Infectious Diseases, Musashimurayama, Tokyo, Japan, **3** Department of Infection and Immunology, Clinical Research Center, National Hospital Organization Nagoya Medical Center, Naka-ku, Nagoya, Aichi, Japan, **4** Department of Microbiology and Molecular Medicine, University of Geneva, Geneva, Switzerland

Abstract

Human immunodeficiency virus (HIV) type 2 shows limited geographical distribution compared with HIV type 1. Although 8 genetic groups of HIV type 2 (HIV-2) have been described, recombinant viruses between these groups are rarely observed. Recently, three HIV-2 patients in Japan were described with rapidly progressive, acquired immunodeficiency. These patients were infected with an A/B inter-group recombinant designated CRF01_AB. Here, we characterize the capsid protein (CA) encoded by the viruses from these patients. HIV-2 CRF01_AB CA showed unique amino acid sequence almost equally distinct from group A and group B viruses. Notably, HIV-2 CRF01_AB CA showed potent resistance to human TRIM5α. In addition to the previously identified amino acid position 119 in the N-terminal domain of CA, we found that HIV-2 CRF01_AB-specific amino acid substitutions in the C-terminal domain also were necessary for resistance to human TRIM5α. These results indicate that retroviruses can evade TRIM5α by substitution at residues within the C-terminal domain of CA.

Citation: Miyamoto T, Nakayama EE, Yokoyama M, Ibe S, Takehara S, et al. (2012) The Carboxyl-Terminus of Human Immunodeficiency Virus Type 2 Circulating Recombinant form 01_AB Capsid Protein Affects Sensitivity to Human TRIM5α. PLoS ONE 7(10): e47757. doi:10.1371/journal.pone.0047757

Editor: Vladimir Brusic, Dana-Farber Cancer Institute, United States of America

Received July 31, 2012; **Accepted** September 20, 2012; **Published** October 19, 2012

Funding: This work was supported by grants from the Health Science Foundation; the Ministry of Education, Culture, Sports, Science, and Technology, Japan (23590541 to EEN, 23390111 to TS), the Ministry of Health, Labour, and Welfare, Japan (H22-AIDS-003 to HS), Swiss National Fund grant 3100A0-128655 to JL, and NIH grant RO1AI59159 to JL. The funders had no role in study design, data collection and analysis, decision to publish, or preparation of the manuscript.

Competing Interests: The authors have declared that no competing interests exist.

* E-mail: shioda@biken.osaka-u.ac.jp

Introduction

Human immunodeficiency virus type 2 (HIV-2) has been detected primarily in West Africa, in contrast to the global distribution of the type 1 epidemic virus (HIV-1). Based on molecular evidence, HIV-2 and HIV-1 are presumed to derive from simian immunodeficiency viruses that originated in sooty mangabey (SIVsm) and chimpanzee (SIVcpz), respectively, as a result of zoonotic transfer between non-human primates and human. The HIV-1 and HIV-2 bear a considerable degree of homology in both gene organization and RNA sequence (30%–60%) [1–4]. It is generally believed that HIV-2 is less pathogenic than HIV-1. However, certain HIV-2 patients with high plasma HIV-2 loads develop acquired immune deficiency syndrome (AIDS) as rapidly as HIV-1 patients do [4]. To date, eight HIV-2 groups have been distinguished on the basis of phylogenetic (sequence) analysis; each group is presumed to have originated from an independent zoonotic event [5].

TRIM5α was identified as a factor that restricts HIV-1 infection in rhesus monkey (Rh) cells [6]. TRIM5α is thought to degrade the core of the incoming virus [7,8]. TRIM5 proteins are members of the tripartite motif family containing RING, B-box, and coiled-coil domains. The alpha isoform of TRIM5 has an additional C-terminal PRYSPRY (B30.2) domain [9]. In cynomolgus monkey (CM), TRIM5α also has been demonstrated to restrict HIV-1 infection [6,10]. In contrast, the human TRIM5α exhibits minimal restriction of HIV-1 infection [11–14], but shows moderate levels of restriction for HIV-2 [15].

Capsid (CA) proteins are components of the viral core; the CAs of HIV-1 and HIV-2 have similar primary and three dimensional structures [16]. CA is composed of a surface-exposed N-terminal domain (NTD) and a C-terminal domain (CTD) that is required for oligomerization [17]. We previously identified a single amino acid of the HIV-2 capsid that determines the susceptibility of HIV-2 to CM TRIM5α. Viruses that encoded CAs with either alanine or glutamine at amino acid residue 119 (which corresponded to the 120th amino acid of the CA of the GH123 viral strain) could grow in cells harboring the CM TRIM5α. In contrast, HIV-2 encoding CA with proline at the same position showed restricted growth in cells harboring the CM TRIM5α. Similar results, although to a lesser extent, were observed when the human TRIM5α was used [15]. Furthermore, an analysis of HIV-2 CA variation in a West African Caio cohort demonstrated that the presence of proline at CA positions 119, 159, and 178 was more frequent in individuals with lower viral loads (VLs); the presence of non-proline residues at all 3 residues was more frequent in

individuals with high VLs. The *in vitro* replication levels of viruses bearing changes at the 3 positions suggested that these 3 residues influence virus replication by altering susceptibility to TRIM5α [18]. These results also suggested that TRIM5α controls virus replication in HIV-2-infected individuals.

Recently, five HIV-2-seropositive cases were identified in Japan. Three isolates (NMC307, NMC716, and NMC842) were recovered from these patients and were shown by full-length genomic analysis to represent a recombinant (designated HIV-2 CRF01_AB) of group A and B strains [19]. Although more than 75% of patients with HIV-2 have asymptomatic prognoses throughout their lifetimes [1,20], all 3 of the CRF01_AB patients were found to be at an advanced stage of AIDS with low CD4+ cell counts and high HIV-2 VLs [19]. All 3 patients were under 40 years of age when first diagnosed as HIV-2 positive [19]. Assessment of risk factors suggested that all three were infected via heterosexual contacts; no personal connection was confirmed among any of these cases [19]. In the present study, we characterized the HIV-2 CRF01_AB CA obtained from these patients and found several unique properties of HIV-2 CRF01_AB, including potent resistance to human TRIM5α-mediated restriction.

Results

HIV-2 CRF01_AB Strains Show Unique CA Sequences

Fig. 1 shows an alignment of the deduced amino acid sequences of the CAs of HIV-2 group A (ROD, UC12, GH123, and UC2), HIV-2 group B (UC14, D205, and UC1), SIVs (SIVmac239 and SIVsm PBJ14), and HIV-2 CRF01_AB (NMC307, NMC716, NMC842, and 7312A). As we reported previously [15,18], the 119th amino acid position is a proline, glutamine, or alanine in the CAs of HIV-2 group A, HIV-2 group B, and SIVs. However, the CAs of the HIV-2 CRF01_AB strains uniquely possess a glycine at this position. Based on the genomic structure of HIV-2 CRF01_AB, A/B recombinant breakpoints within this isolate are located near or within the *env* gene, such that HIV-2 CRF01_AB can be considered to consist of a group B backbone that incorporates group A *env* fragments [19]. These presumed breakpoints could be taken to suggest that CRF01_AB CA should be encoded as a B-like sequence. However, phylogenetic analysis of these CA sequences (Fig. 2) reveals that the deduced HIV-2 CRF01_AB CA proteins constitute a distinct cluster, with the dendrogram exhibiting a long branch length compared to the CAs of HIV-2 group A, HIV-2 group B, and SIV.

HIV-2 CRF01_AB CA is Highly Resistant to Human TRIM5α

In a previous study, we reported that the amino acid at residue 119 of the HIV-2 CA affects susceptibility to the restriction of virus replication by CM and human TRIM5α [15], such that HIV-2 encoding CA(Pro119) was sensitive to CM and human TRIM5α, while HIV-2 encoding CA(Gln119) or CA(Ala119) was resistant [15]. We also reported that mutation of HIV-2 strain GH123 to encode glycine at the corresponding position (GH123/G) rendered GH123 resistant to CM TRIM5α [21]. To further test the role of the CA protein in TRIM5α resistance, we generated recombinant versions of the GH123 virus (716 or 842) in which the CA-encoding segment of *gag* was replaced with that of the A/B recombinants NMC716 or NMC842 (respectively). We used a recombinant Sendai virus (SeV) system to express CM, Rh, and human TRIM5α and CM TRIM5α lacking the PRYSPRY domain as a negative control (Fig. S1). In the presence of CM TRIM5α, infection by the parental GH123 virus was restricted, but infection by GH123/G was resistant to CM TRIM5α-mediated restriction (Fig. 3A). Infection by 716 or 842 was resistant to CM TRIM5α (Fig. 3B). In contrast, infection by any of the 4 variants (GH123, GH123/G, 716, and 842) was completely restricted by Rh TRIM5α (Fig. 3A, B). These results for cells producing CM or Rh TRIM5α are consistent with our previous findings [22]. In cells producing human TRIM5α, the replication of parental GH123 and of the GH123/G mutant were partially restricted (Fig. 3A), while 716 and 842 replicated as efficiently as in negative control cells that did not produce a functional TRIM5α (Fig. 3B). The mean ratios of the p25 levels at 6 days after infection in the cells producing human TRIM5α to those in the negative control cells were 0.14 for GH123, 0.30 for GH123/G, but 0.81 for 716 and 1.02 for 842 in three independent experiments. The ratio of GH123/G was significantly higher than that of GH123 ($P = 0.0086$, t test) but lower than those of 716 ($P = 0.0059$, t test) and 842 ($P = 0.0030$, t test). Similar results were obtained when we calculated the mean ratios of the p25 levels at 3 days after infection (data not shown). These data indicate that the CA sequences of the CRF01_AB strains conferred higher potential to escape from human TRIM5α than those of GH123/G.

Viral Sensitivity to Human TRIM5α-mediated Restriction in a Single Round Infection Assay

TRIM5α restricts viral infection at a post-entry step [6,23,24]. To focus on early steps of virus replication, we performed a single-round infection assay, in which infection is detected as fluorescence generated by production of the green fluorescent protein (GFP). To construct mutant viruses encoding GFP, the fragment of GH123, 842, or GH123/G that encoded the matrix (MA) and CA proteins was transferred to the *env*-disrupted HIV-2 genomic clone pROD-env(-)-GFP, which directs the production of GFP after infection [25]. Vesicular stomatitis virus glycoprotein (VSV-G) pseudotyped wild-type and mutant HIV-2 GFP viruses were inoculated into feline CRFK cells producing TRIM5α, and GFP-positive cells were counted 2 days after infection. In this experiment, we used feline cells, since feline cells lack expression of endogenous TRIM5α. In the presence of CM TRIM5α, the numbers of GFP-positive cells were greater in cells infected with GFP-expressing viruses encoding the GH123/G or 842 CAs than in those infected with the GFP-expressing viruses encoding GH123 CA (Fig. 4), confirming that viruses encoding CA(G119) were resistant to CM TRIM5α. Consistent with the results shown in Fig. 3B, the GFP-expressing virus encoding the 842 CA from a patient was more resistant to human TRIM5α-mediated restriction than viruses encoding the CAs from GH123 ($P = 0.0010$, t-test) or GH123/G ($P = 0.0026$, t-test) (Fig. 4).

Viral Growth in TRIM5α Knock-down Cells

We next investigated whether the different resistance to human TRIM5α restriction among recombinant HIV-2 strains still applied in cells producing physiological levels of human TRIM5α protein. For this purpose, we used TRIM5α "knock-down" Jurkat cells (TRIM5α-KD Jurkat) and the corresponding control Jurkat line (Luci-siRNA Jurkat) [26]. It was demonstrated that the level of TRIM5α mRNA in TRIM5α-KD Jurkat is five times lower than that of Luci-siRNA Jurkat by TaqMan quantitative PCR. Three days after infection, GH123 replicated better in TRIM5α-KD Jurkat than in Luci-siRNA Jurkat (Fig. 5A). On the other hand, GH123/G, 716, and 842 yielded comparable titers in both cell lines (Fig. 5B, 5C, and 5D). In this experiment, we found that GH123/G also was resistant to human TRIM5α. Nevertheless, the data presented in Fig. 5 indicated that GH123 was sensitive to human TRIM5α produced at physiologically relevant levels, while 716 and 842 possessed potent resistance against human TRIM5α.

```
HIV-2A   ROD      PVQHVGG-NYTHIPLSPRTLNAWVKLVEEKKFGAEVVPGFQALSEGCTPYDINQMLNCVG  59
         UC1      ...Q.A.-....V.....................................................  59
         GH12     ...QT..G..I.V..............D.....................................  60
         UC2      ...QA..-..V.V.....................................................  59
HIV-2B   UC14     ...QIA.-..S.L.....................................................  59
         D205     ...QLA.-..V.L.....................................................  59
         UC1      ...QIA.-..V.M.....................................................  59
SIV      mac239   ...QI..-..V.L............I.........................................  59
         PBJ14    ...QI..-....L............I.........................................  59
HIV-2AB  NMC307   ...Q.A.-..V.V.....................I.............................  59
         NMC716   ...Q.A.-..V.V.....................I.............................  59
         NMC842   ...Q.A.-..V.V.....................I.............................  59
         7312A    ...Q.A.-..V.V..................L..............................  59

                                                                          119
                                                                           ↓
HIV-2A   ROD      DHQAAMQIIREIINEEAAEWDVQHPIPGPLPAGQLREPRGSDIAGTTSTVEEQIQWMFRP  119
         UC12     ..................D.........................................  119
         GH123    ..............D...D..A..............D...................Y..  120
         UC2      .Q................D..A..............D.............D......Y.Q  119
HIV-2B   UC14     E.................D..Q...S...M.........................Y.A  119
         D205     E.................D..Q...S...M......D..................Y.A  119
         UC1      ..................D..Q..............D..................Y.A  119
SIV      mac239   ..........D.......D..L...Q.A.QQ-......S.........S.D......Y.Q  118
         PBJ14    E.................D..L...Q...I.P..................D......Y.Q  119
HIV-2AB  NMC307   E......V..........D..Q...V..........D............P.......Y.G  119
         NMC842   E......V..........D..Q..............D...................Y.G  119
         NMC716   E......V..........D..Q..............D...................Y.G  119
         7312A    E......V..........D..Q...V..........D...................Y.G  119

                                                  159        HindIII  178
                                                   ↓           ↓       ↓
HIV-2A   ROD      QNPVPVGNIYRRWIQIGLQKCVRMYNPTNILDIKQGPKEPFQSYVDRFYKSLRAEQTDPA  179
         UC12     ..............................................................  179
         GH123    ..............................V...............................  180
         UC2      ............................V..V......S................A...  179
HIV-2B   UC14     ..............L...............................................  179
         D205     ..............L...............................................  179
         UC1      ..............................................................  179
SIV      mac239   ...I..........L..............V.........................A.  178
         PBJ14    ...I..........L..............V..................S........  179
HIV-2AB  NMC307   ..SI..........L..............V.......................A.T.  179
         NMC716   ..S...........L..............V........................Q.  179
         NMC842   ..S...........L..............V.......................A.T.  179
         7312A    .S.I..........L..............V.......................A.T.  179


HIV-2A   ROD      VKNWMTQTLLVQNANPDCKLVLKGLGMNPTLEEMLTACQGVGGPGQKARLM  230
         UC12     ..........I..................G.........................  230
         GH123    ..........I...................................          231
         UC2      ..............................................          230
HIV-2B   UC14     ..........I..............................I..........  230
         D205     ..........I..............................I..........  230
         UC1      ..........I..............................I..........  230
SIV      mac239   ..........I..............V.........................  229
         PBJ14    ..........I..............I.........................  230
HIV-2AB  NMC307   .RA...E..................PH............I..........  230
         NMC716   .RA...E...I..............PH............I..........  230
         NMC842   .RA...E..................PH............I..........  230
         7312A    .RA...E..................PH............I..........  230
```

Figure 1. Alignments of amino acid sequences of CA proteins encoded by selected HIV-2 isolates and SIV from the Los Alamos databases. Dots denote amino acid identity with the ROD CA; dashes denote gaps introduced to optimize alignment. HIV-2 CRF01_AB-specific amino acid residues are in red. Arrows indicate key residues at 119, 159, and 178, and the position (in the corresponding DNA sequence) of the *Hind*III restriction site used in the constructs. HIV-2A, HIV-2B, and HIV-2AB denote HIV-2 group A, HIV-2 group B, and HIV-2 CRF01_AB, respectively.
doi:10.1371/journal.pone.0047757.g001

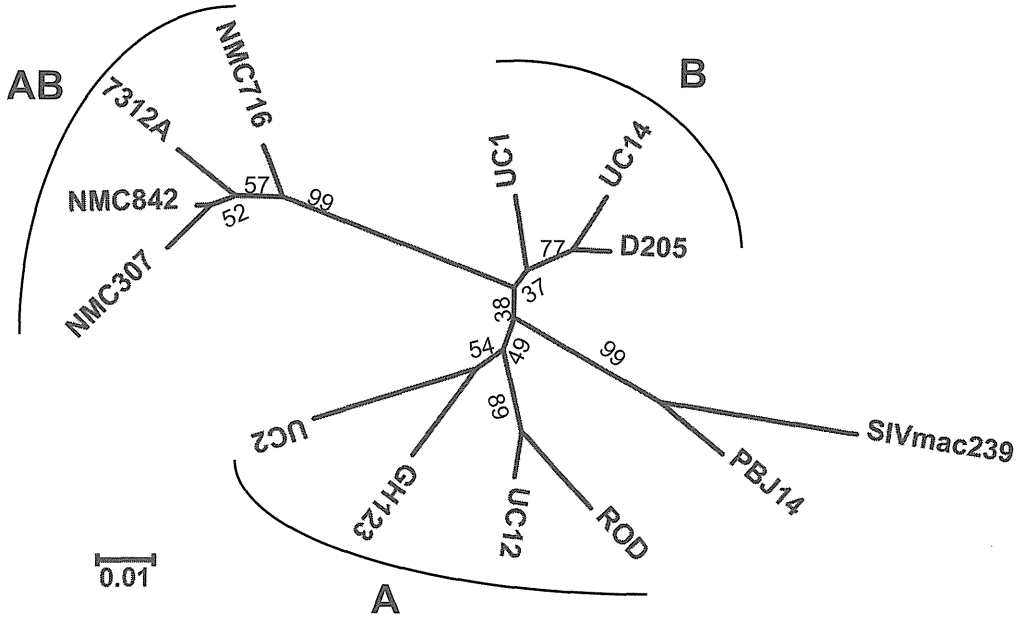

Figure 2. Phylogenetic tree of HIV-2 isolates and SIV. This phylogenetic tree was constructed by the neighbor-joining method. Bootstrap probabilities (%), as calculated by 1000 iterations, are shown at the major tree nodes. Scale bar represents 0.01 amino acid substitutions per site. A, B, and AB denote HIV-2 group A, HIV-2 group B, and HIV-2 CRF01_AB, respectively.
doi:10.1371/journal.pone.0047757.g002

Since TRIM5α-KD Jurkat always showed reduced proliferative properties compared to Luci-siRNA Jurkat (data not shown), presumably due to reduced TRIM5α levels [27], the p25 levels of all these viruses in Luci-siRNA Jurkat became higher than those in TRIM5α-KD Jurkat at 10 days after infection (data not shown).

HIV-2 CRF01_AB CA C-terminal Domain-specific Sequence also Affects Viral Sensitivity to Human TRIM5α

We previously reported that the presence of proline at CA positions 119, 159, and 178 is more frequent in individuals with lower VLs [18]. Viral isolates NMC307, NMC716, and NMC842 all encoded CAs with proline at the 159th position (Fig. 1). However, the 178th amino acid residue was encoded as a threonine (NMC307 and NMC842) or as a glutamic acid (NMC716) in these isolates (Fig. 1). To test whether a single residue at amino acid 178 of HIV-2 CRF01_AB CA affects the sensitivity to human TRIM5α, we generated recombinant 716 or 842 viruses (designated 716GPP or 842GPP, respectively) that encoded CA (Pro178) proteins. As shown in Fig. 3C, 716GPP and 842GPP escaped from human TRIM5α restriction as efficiently as 716 and 842 did. These data suggest the existence of viral determinants for human TRIM5α-resistance other than the previously identified 119th and 178th amino acid positions of CA.

To search for the viral determinants of human TRIM5α resistance other than the 119th and 178th amino acid positions of HIV-2 CA, we constructed a chimeric virus 842Hind by replacing the segment of the 842 genome that encodes CA C-terminal residues 170 to 231 with the corresponding region of GH123 (Fig. 6A). When tested in cells that produced human TRIM5α, 842 was strongly resistant to human TRIM5α as expected (Fig. 6B). However, the 842Hind construct, which encoded the NMC842 CA with the GH123 CA C-terminal short region, lost this resistance to human TRIM5α (Fig. 6C). The mean ratios of the p25 levels at 6 days after infection in the cells producing human TRIM5α to those in the negative control cells were 0.73 for 842 and 0.16 for 842Hind in three independent experiments. The ratio of 842Hind was significantly lower than that of 842 ($P = 0.0003$, t test). Similar results were obtained when we calculated the mean ratios of the p25 levels at 3 days after infection (data not shown). These results suggest that one or more of the HIV-2 CRF01_AB-specific amino acid residues within the CA C-terminal short region (Fig. 1, shown in red) also are necessary to fully evade human TRIM5α.

Molecular Dynamics of N-terminal Domain (NTD) of HIV-2 CRF01_AB CA

Residue 120 of the GH123 CA, which corresponds to residue 119 of the CRF01_AB CA, is located in the loop between α-helices 6 and 7 (L6/7) of CA NTD. Our previous molecular dynamics simulation study of HIV-2 CA NTD revealed that mutations at this position affected conformation of the neighboring loop between α-helices 4 and 5 (L4/5), and TRIM5α-sensitive viruses were predicted to share a common L4/5 conformation. In addition, the shared L4/5 structures of the sensitive viruses were associated with a decreased probability of hydrogen bond formation between GH123 CA's Asp97 (in L4/5) and Arg119 (corresponding to residue 118 in HIV-2 CRF01_AB CA; in L6/7) [21]. TRIM5α-resistant viruses exhibited a variable L4/5 conformation and a higher probability of hydrogen bond formation between L4/5 and L6/7 [21]. As noted above, HIV-2 CRF01_AB strains have a unique Gly119 (Fig. 1), which we had not previously modeled by molecular dynamics simulation. Therefore, three-dimensional (3-D) models of HIV-2 GH123/G and NMC842 CA NTD were constructed using homology modeling based on the crystal structures of the HIV-2 CA NTD, and the models were subjected to molecular dynamics simulation to compare the results with those derived from previously constructed 3-D structural models of TRIM5α-sensitive GH123 and TRIM5α-resistant GH123/Q and GH123/A [21]. GH123/Q and GH123/A encode CA (Gln120) and CA (Ala120), respectively [15]. Contrary to our expectation, the predicted L4/5 conformations of the NTDs of the NMC842 CA and GH123/G CA differed from those of

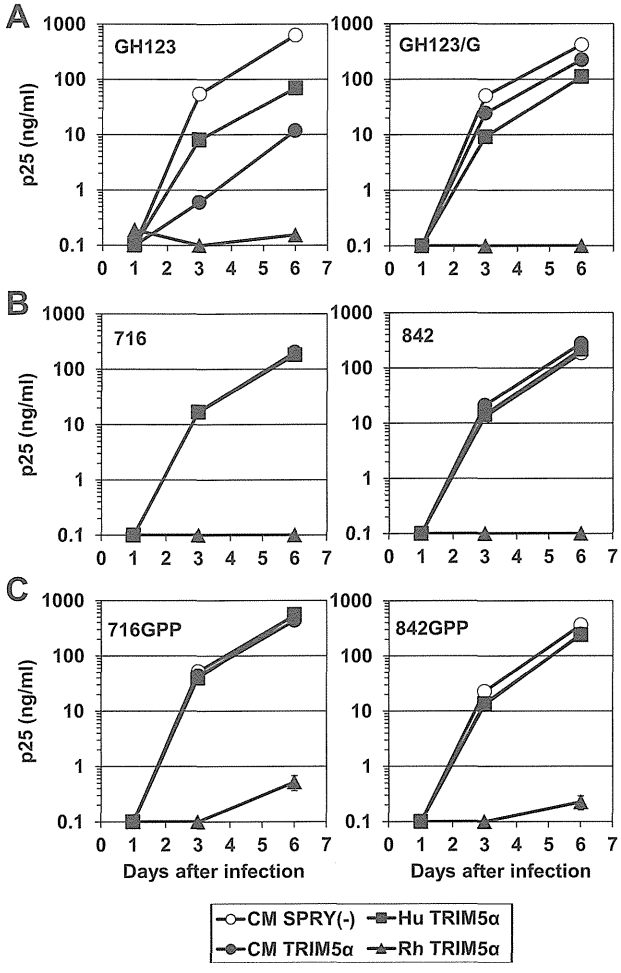

Figure 3. Growth of HIV-2 strain GH123 and variants thereof in the presence of TRIM5α. (A), (B), (C) Virus levels were measured by ELISA detection of p25 (CA) levels in supernatants. CEM-SS cells were infected with recombinant SeV encoding rhesus (Rh: black triangles); cynomolgus monkey (CM: black circles); human (Hu: black squares); or CM SPRY(-) (white circles) TRIM5α. CM SPRY (-) has a dominant negative effect on the anti-viral activity of TRIM5α and serves as a negative control. Nine hours after infection, cells were superinfected with GH123, GH123/G, 716, 842, 716GPP, or 842GPP. Error bars show actual fluctuations between levels of p25 (CA) in duplicate samples from one of three independent experiments.
doi:10.1371/journal.pone.0047757.g003

TRIM5α-resistant GH123/Q and GH123/A, better resembling that predicted for the CA NTD encoded by TRIM5α-sensitive GH123 (Fig. 7). Indeed, the calculated probability of hydrogen bond formation between L4/5 and L6/7 was even lower for the CAs of GH123/G (20.80%) and NMC842 (30.58%) compared to that of GH123 (44.6%). These results suggest that Gly119 endows the CRF01_AB CA NTD with unique structural properties.

Steric Locations of HIV-2 CRF01_AB-specific Amino Acid Substitutions

As noted above, HIV-2 CRF01_AB strains have several specific amino acid substitutions at the C-terminal domain (CTD) of CA (Fig. 1, shown in red); these substitutions were necessary for the potent resistance of these isolates against human TRIM5α (Fig. 6). Previously, we suggested that magnitudes of the computationally calculated binding energies of the CA CTD dimer models tend to be significantly greater in the TRIM5α-less-sensitive HIV-2s in

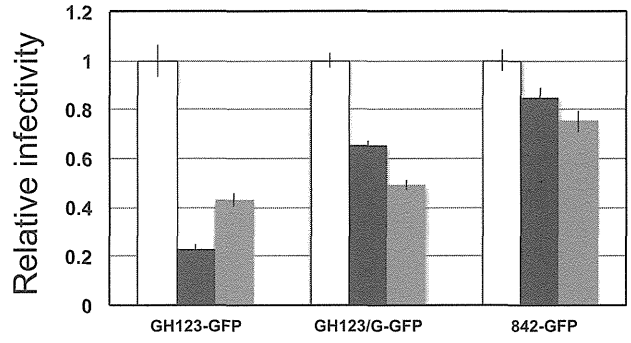

Figure 4. Viral sensitivity to TRIM5α-mediated restriction in a single-round infection assay. Feline CRFK cells were infected with SeV encoding cynomolgus monkey (CM; black bars), human (grey bars), or CM SPRY(-) (white bars) TRIM5α. CM SPRY (-) has a dominant negative effect on the anti-viral activity of TRIM5α and serves as a negative control. The cells then were superinfected with a green fluorescent protein (GFP)-expressing virus, GH123-GFP, GH123/G-GFP, or 842-GFP containing 500ng of p25 (CA). Two days after infection, the cells were fixed by formaldehyde, and GFP-producing cells were counted by flow cytometry. Numbers of GFP-positive cells in CM SPRY (-)-producing cells are set at one and relative numbers to CM SPRY (-) of GFP-positive cells are shown. Error bars denote standard deviations of triplicate samples from one of three independent experiments.
doi:10.1371/journal.pone.0047757.g004

West Africa [18]. To examine if the HIV-2 CRF01_AB-specific amino acid substitutions in CA CTD could influence the CTD-CTD dimer stability, we constructed the CA CTD dimer model of HIV-2 CRF01_AB NMC842 by homology modeling and analyzed steric locations of the specific substitutions and binding energies of the CTD dimer model. In the CA CTD dimer model of NMC842, HIV-2 CRF01_AB-specific amino acid substitutions are located in helix 9 and in the loop between helices 10 and 11, and all appeared to be situated near but distinct from the CTD-CTD dimer interface (Fig. 8A). The predicted binding energy of the CTD-CTD dimer model of the NMC842 isolate (79.6 kcal/mole) was similar to that reported in TRIM5α sensitive viruses [18]. The results may imply that the HIV-2 CRF01_AB-specific amino acid substitutions in CTD do not necessarily influence the CTD-CTD dimer stability of the TRIM5α sensitive virus.

To further obtain structural insights into the roles of these CRF01_AB-specific mutations, we analyzed their steric locations in the CA hexamer. In the hexamer model of GH123 CA that we previously constructed based on the HIV-1 CA hexamer [28], HIV-2 CRF01_AB-specific amino acid substitutions in CTD form clusters and are located at the outermost part of the hexamer (Fig. 8B and C). Notably, these substitutions exist directly under the L4/5 of neighboring CA (Fig. 8C), and most of them are clearly visible from right above (Fig. 8B). These results raise a possibility that HIV-2 CRF01_AB-specific amino acid substitutions in CA CTD may be exposed to and accessible from the outside of the viral core.

Discussion

In the present study, we have shown that the CA of HIV-2 CRF01_AB isolates have a unique feature distinct from that of other HIV-2 strains; CRF01_AB-specific sequences conferred strong resistance to human TRIM5α. In addition to the previously identified role of amino acid 119 of the CA NTD, CRF01_AB-specific amino acid substitutions in the CA CTD also were necessary for strong resistance to human TRIM5α. These amino

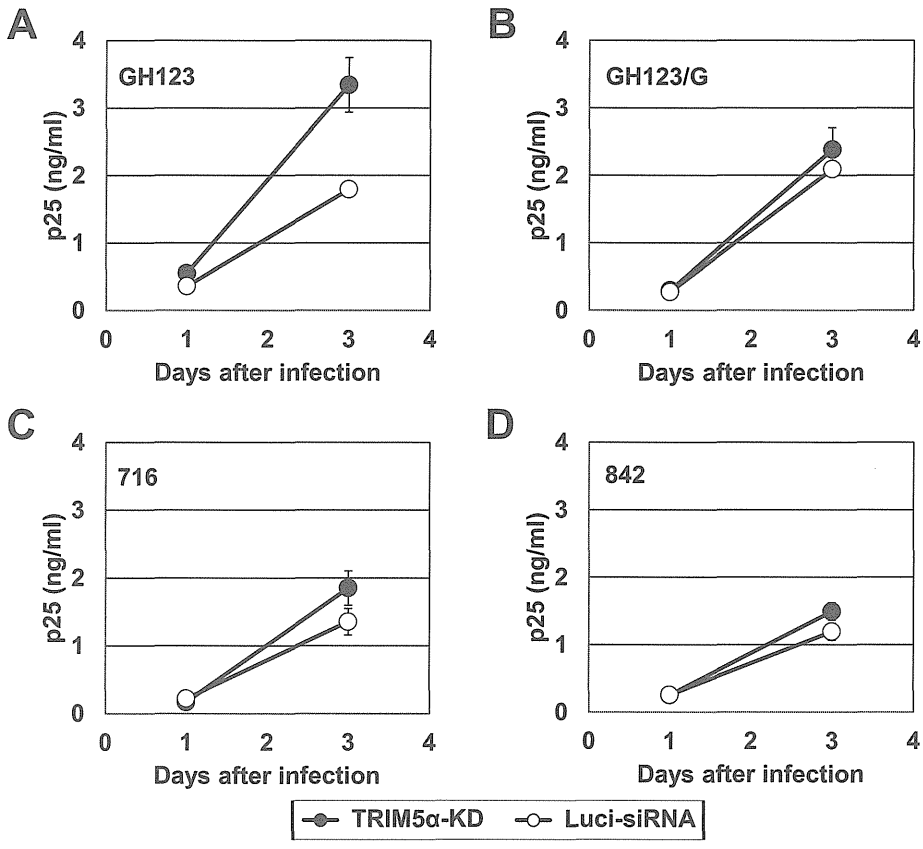

Figure 5. Viral growth in TRIM5α knock-down cells. (A), (B), (C) and (D) TRIM5α-KD Jurkat ("knock-down") or Luci-siRNA Jurkat (control) cells were infected with derivatives of GH123 virus. Culture supernatants were periodically assayed for levels of virus capsid. Error bars show actual fluctuations of duplicate samples from one of two independent experiments. Black and white bars denote TRIM5α-KD Jurkat and Luci-siRNA Jurkat cells, respectively.
doi:10.1371/journal.pone.0047757.g005

acid substitutions in CA CTD may be exposed to and accessible from the outside of the viral core.

Retroviral CA is known to form hexamers [29]. The CTD domain of retroviral capsid protein participates in CA dimerization, where intermolecular CTD-CTD interactions are mediated by symmetric, parallel dimerization of helix 9 from the CTD domains of adjacent hexamers [30]. This dimerization process is prerequisite for assemblies of multiple hexamers [29]. Previously, we found that the computationally calculated binding energies of the CA CTD dimer models could have positive relations with the TRIM5α susceptibilities of HIV-2s in West Africa [18]. We therefore calculated here the binding energy of the CTD-CTD dimer model of the NMC842 using computational method. However, the predicted binding energy of the CTD-CTD dimer of the NMC842 isolate was rather similar to that reported in TRIM5α sensitive viruses [18]. Therefore, previously undescribed mechanisms may be involved in the TRIM5α resistance of the HIV-2 CRF01_AB.

A possible mechanism for the findings may be that the CRF01_AB-specific substitutions influence directly or indirectly the structural properties of an interaction surface for the TRIM5α mediated inhibition. In this regard, we previously suggested with SIV that not only the NTD but also the CTD might constitute an intermolecular interaction surface [31]. Similarly, HIV-2 may have such interaction surface in CTD domain, and the surface may be used for the TRIM5α-mediated inhibition. Results on the steric locations of the CRF01_AB-specific substitutions in the hexamer model support this possibility (Fig. 7B and C). A preliminary modeling study of the assemblies of the CA hexamers also have supported this possibility: the NTDs are apart from each other among the hexamers, which allows to form accessible surface on the CTDs (data not shown), as suggested with Rous sarcoma virus CA [32]. Therefore, it would be interesting to examine whether HIV-2 CRF01_AB-specific amino acid substitutions in CTD could constitute a binding cleft for the TRIM5α itself or others involved in TRIM5α medicated inhibition in the assemblies of multiple CA hexamers in the viral core. Further study is necessary to address this issue.

Previously, we showed that the amino acid replacements at CA residue 119 affected the conformation of the neighboring L4/5, and that TRIM5α-sensitive viruses had a shared L4/5 conformation that was associated with a decreased probability of hydrogen bonding between L4/5 and L6/7 [21]. Although GH123/G and 842 showed resistance to TRIM5α, the calculated probability of hydrogen bond formation between L4/5 and L6/7 was lower than that calculated for the CAs of other TRIM5α-resistant viruses, including that from GH123/Q (55.15%) and GH123/A (64.47%) [21]. The conformations of L4/5 in the CAs of GH123/G and 842 also were similar to those of TRIM5α-sensitive viruses, and were distinct from those of the CAs of TRIM5α-resistant viruses. These characteristics of GH123/G and 842 were similar to those of GH123/E and GH123/D, mutant GH123 clones encoding glutamic acid and aspartic acid (respectively) at the residue corresponding to

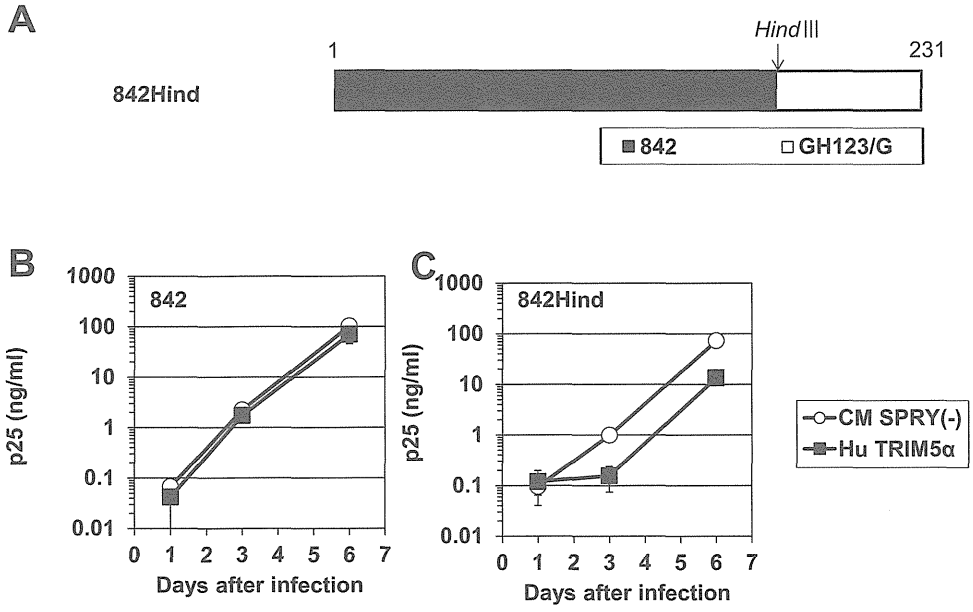

Figure 6. HIV-2 CRF01_AB CA C-terminal domain-specific sequence also affects viral sensitivity to human TRIM5α. (A) Schematic representation of chimeric viral CAs. Black and white bars show 842 and GH123/G CA peptide sequences, respectively. An arrow denotes the position (in the corresponding DNA sequence) of the *Hind*III restriction site used in the construct. (B and C) CEM-SS cells were infected with recombinant SeV encoding human (Hu: black squares) or CM SPRY(-) (white circles) TRIM5α. Nine hours after infection, cells were superinfected with 842 (B) and 842Hind (C). Culture supernatants were assayed for levels of p25 (CA). Error bars show actual fluctuations between levels of p25 (CA) in duplicate samples from one of three independent experiments.
doi:10.1371/journal.pone.0047757.g006

position 119 of HIV-2 CRF01_AB strains [21]. Although glutamic acid and aspartic acid have not been observed at this CA residue in HIV-2 isolated clinically, both GH123/E and GH123/D showed resistance against CM TRIM5α. In contrast to the CAs of GH123/Q and GH123/A, the CAs of both GH123/E and GH123/D show reduced likelihoods of hydrogen bond formation between the L4/5 and L6/7, and the L4/5 conformations were predicted to be similar to those of the CAs of TRIM5α-sensitive viruses. Therefore, our present results extend our previous observations, and additionally imply that the Gly119 of HIV-2 CRF01_AB CA prevents binding by TRIM5α, probably due to the small size of the glycine side chain. It is possible that the shared conformation of L4/5 might have some advantages in utilizing certain cellular factor(s) that bind CA. Our structural data suggests that HIV-2 CRF01_AB strains are highly adapted, since these strains have acquired potent resistance against TRIM5α without losing the shared L4/5 conformation.

In the case of GH123/E, disruption of the hydrogen bond between L4/5 and L6/7 by substitution of alanine for aspartic acid at position 97 (D97A) did not alter the resistant phenotype of GH123/E [21], while the same substitution almost completely abolished the replicative ability of GH123/G (data not shown). This result further demonstrates the unique status of GH123/G, since D97A substitution did not cause such a drastic reduction of replicative ability in GH123, GH123/Q, and GH123/A [21]. The basis for the difference between GH123/G and other variants is unclear; further mutational studies will be necessary to elucidate detailed interactions between L4/5 and L6/7, and to define the contribution of these sequences to viral replication and TRIM5α sensitivity.

In the Los Alamos databases, almost all SIV isolates encode glutamine at the position corresponding to residue 119 of the HIV-2 CRF01_AB CA. It is likely that the sequential mutation from glutamine (coded as CAA or CAG) to proline (CCA or CCG; underlines denote single nucleotide changes) and then to alanine (GCA, GCG) occurred after transmission of the monkey virus to the human population. The nature of the genetic code suggests that the Gly119-encoding virus (GGA or GGG codon) derived from the Ala119-encoding virus, implying that the viruses with glycine are highly adapted, as also discussed above. A single HIV-2 strain encoding glycine at the 119th CA residue was found in the Los Alamos databases; this strain (7312A) was isolated from a symptomatic 32-years-old man [33], and also was a recombinant between groups A and B (Fig. 1 and 2). This recombinant virus exhibits a genomic organization similar to that of NMC307, NMC716, and NMC842. At present, we do not know whether the emergence of glycine at the 119th position of CA is unique to HIV-2 CRF01_AB. It will be critical to assess the emergence of Gly119 viruses within HIV-2 groups A and B.

It is generally believed that HIV-2 is less pathogenic than HIV-1, and the number of HIV-2 cases is now gradually decreasing in West Africa. However, NMC307, NMC716, and NMC842 were recovered from patients at an advanced stage of AIDS with low CD4+ cell counts and high HIV-2 VLs [19]. It is possible that these HIV-2 CRF01_AB strains are highly pathogenic, unlike other HIV-2 strains. Careful epidemiological and virological studies are necessary to test this hypothesis. In the present study, we found that HIV-2 CRF01_AB CA confers strong resistance to human TRIM5α. In the Caio HIV-2 cohort in West Africa, non-proline residues at position 119 were significantly associated with elevated plasma HIV-2 load [18]. Therefore, resistance to TRIM5α may at least partially explain why these 3 patients in Japan developed AIDS so rapidly, although the possible effects of mutations in regions (e.g., *env*, *vif*, *nef* and the long terminal repeats) other than those that encode CA cannot be fully excluded at

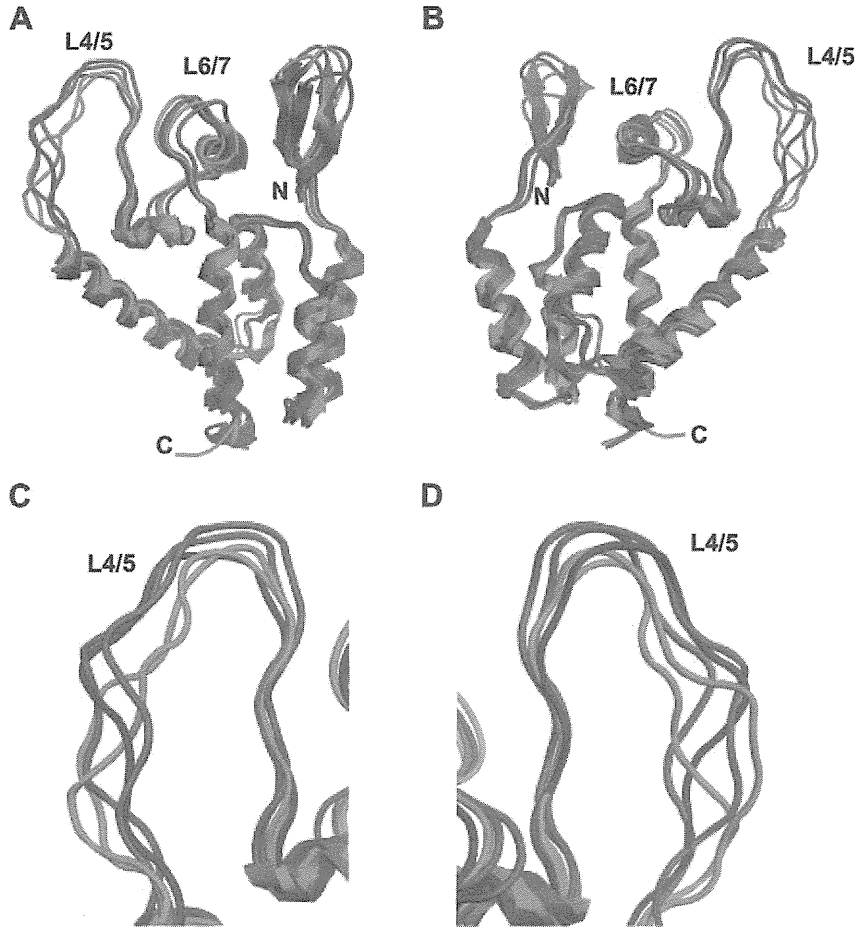

Figure 7. Structural models of the HIV-2 capsid N-terminal domain. Models were constructed by homology modeling and molecular dynamics simulations with the high-resolution X-ray crystal structure of the HIV-2 capsid N-terminal domain (CA NTD) (PDB code: 2WLV [16]) as the starting structure. Averaged conformations of the overall structure of the CA NTD (from the amino acid position 1 to 150) during 5–20 nanoseconds of MD simulations (A and B) and a close-up view around the L4/5 loop (C and D) are indicated. N and C indicate the amino termini and carboxyl termini, respectively. Models are color coded as follows: red, 842; blue, GH123/G; green, CM TRIM5α-resistant viruses (GH123/Q and GH123/A); and purple, CM TRIM5α-sensitive virus (GH123/P).
doi:10.1371/journal.pone.0047757.g007

present. Our results also suggest that resistance to TRIM5α might be a new marker for the pathogenic potential of HIV-2. The possible emergence of a highly pathogenic HIV-2 strain is an ongoing concern, given that retroviruses can easily evolve to evade host defenses.

Materials and Methods

Phylogenetic Tree Analysis

Multiple sequence alignment was performed using the software CLUSTALW version 2.1. Phylogenetic trees were constructed using the neighbor-joining method. Bootstrap probabilities were calculated by 1000 iterations [34].

Cell Culture

The human 293T [35] and feline CRFK [36] cells were maintained in Dulbecco's Modified Eagle medium. The human T-cell line CEM-SS [37] was maintained in RPMI medium. All media were supplemented with 10% fetal bovine serum and 1% penicillin-streptomycin.

Plasmid Construction

Recombinant HIV-2 GH123 clones containing the entire CA sequence of the isolates NMC716 or NMC842 (716 or 842, respectively) and 716 or 842 with proline substitutions at the 178th position (716GPP or 842GPP, respectively) were generated by PCR-based mutagenesis. The GH123/G virus was described previously [21]. The 0.6-kb *Hind*III-*Xho*I fragment of 842 was replaced with the corresponding fragment of GH123/G, and the resulting plasmid was designated 842Hind. Infectious viruses were prepared by transfection of 293T cells with the resulting proviral DNA clones. Viral titers were determined by measuring P25 (CA) with a RetroTek antigen ELISA kit (ZeptoMetrix, Buffalo, NY).

To construct the wild-type and mutant HIV-2 clones encoding GFP, the 1.6-kb *Kpn*I-*Xho*I fragment (which encodes the MA, CA and p6) of GH123, 842, or GH123/G, was transferred to pROD-env(-)-GFP [25], a clone in which the *env* gene is disrupted, and the GFP gene was inserted into the *nef* region. Infectious viruses were prepared by transfection of 293T cells with proviral DNA clones together with the pMD2G plasmid encoding VSV-G. Viral titers were determined as above.

Construction of recombinant SeV encoding C-terminally HA-tagged CM TRIM5α (CM-TRIM5α-SeV), Rh TRIM5α (Rh-

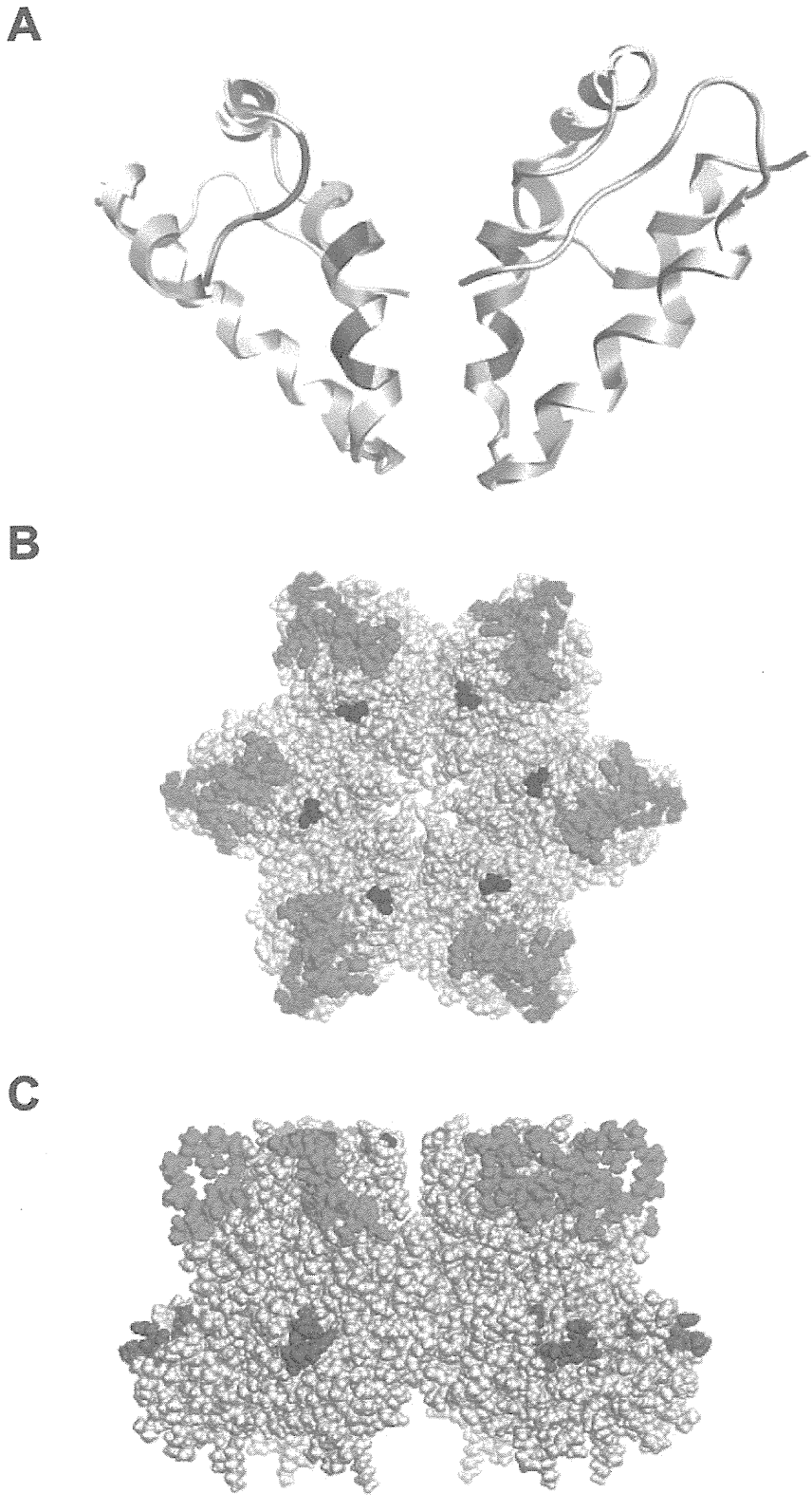

Figure 8. Structural models of the HIV-2 capsid C-terminal domain in dimeric form (A) and the HIV-2 GH123 capsid hexamer (B and C). (A) The C-terminal domain dimer model (from the amino acid position 150 to 219) of HIV-2 capsid (CA) is based on the viral sequence of NMC842. HIV-2 CRF01_AB-specific amino acid substitutions are shown in red. (B and C) The space-filling model of CA hexamer from the top (B) and side (C) is shown. Positions of HIV-2 CRF01_AB-specific amino acid substitutions are shown in red. L4/5 and 120P are shown in green and blue, respectively.
doi:10.1371/journal.pone.0047757.g008

TRIM5α-SeV), human TRIM5α (Hu-TRIM5α-SeV), and CM TRIM5α lacking the PRYSPRY domain (CM-SPRY(-)-SeV) were described previously [10,15,22].

Viral Infection

CEM-SS cells (1×10^6) were infected with SeVs encoding the respective TRIM5α proteins at a multiplicity of infection of 10 plaque-forming units per cell and incubated at 37°C for 9 h. Aliquots of 1×10^5 cells were then superinfected with GH123, GH123/G, 716, 716GPP, 842, 842GPP, or 842Hind virus. Each superinfection used a titer of virus corresponding to 20 ng of p25 (CA). Experiment was performed three separate times with duplicate samples. For viral infection of cells producing physiological levels of TRIM5α, TRIM5α knock-down Jurkat cells (TRIM5α-KD Jurkat) and control cells (Luci-siRNA Jurkat) were infected with GH123, GH123/G, 716, or 842 virus. Each infection used a titer of virus corresponding to 100 ng of p25. The culture supernatants were collected periodically, and the level of p25 (CA) was measured as described above. Experiment was performed two separate times with duplicate samples.

Western Blot

CEM-SS cells (1×10^6) infected with recombinant SeVs expressing HA-tagged TRIM5α proteins were lysed in lysis buffer (50 mM Tris-HCl, pH 7.5, 150 mM NaCl, 1% Nonidet P40, 0.5% sodium deoxycholate). TRIM5α proteins in the lysates were subjected to sodium dodecyl sulfate-polyacrylamide gel electrophoresis. Proteins in the gel were then electronically transferred onto a membrane (Immobilon; Millipore, Billerica, MA). Blots were blocked and probed with anti-HA high-affinity rat monoclonal antibody (Roche, Indianapolis, IN) overnight at 4°C. Blots were then incubated with peroxidase-conjugated anti-rat IgG (American Qualex, San Clemente, CA), and bound antibodies were visualized with a Chemilumi-One chemiluminescent kit (Nacalai Tesque, Kyoto, Japan).

Single-round Infection Assay

SeV-infected CRFK cells (4×10^4) were infected with a titer of pROD-env(-)-GFP derivative virus corresponding to 500 ng of p25 (CA). Two days after infection, the cells were fixed by formaldehyde, and GFP-producing cells were counted by flow cytometry. Experiment was performed three separate times with triplicate samples.

Molecular Modeling and MD Simulation

We used molecular dynamic (MD) simulations [38] to analyze the structural dynamics of the HIV-2 CA NTDs. First, initial CA structures for MD simulation were constructed by homology modeling [39] using the Molecular Operating Environment, MOE (Chemical Computing Group Inc., Montreal, Canada) as described previously [15,40]. We used the high-resolution crystal structure of the HIV-2 CA NTD at a resolution of 1.25Å (PDB code: 2WLV) [16] as the modeling template. Structural dynamics of these HIV-2 CA models in an aqueous environment were analyzed using MD simulations with the SANDER module in the AMBER 9 program package [41] and the AMBER99SB force field with the TIP3P water model [42]. Bond lengths involving hydrogen were constrained with SHAKE [43] and the time step for all MD simulations was set to 2 fs. After heating calculations for 20 ps to 310 K using the NVT ensemble, the simulations were executed using the NPT ensemble at 1 atm and 310 K for 20 ns. Hydration analyses were performed using the ptraj module in AMBER. A maximum cut-off angle of 120.0° and cut-off length of 3.5 Å were used in hydrogen bond definitions.

For the CTD dimer model of HIV-2 CRF01_AB NMC842, a crystal structure of the HIV-1 CA protein was used as the template for the modeling; the dimer of CA C-terminal domain at a resolution of 1.70 Å (PDB code: 1A8O) [17]. The amino acid sequence identity of HIV-1 (1A8O) and HIV-2 CA (NMC842 in this study) is about 76%. The sequence similarity is sufficient to construct a structural model with an r.m.s. deviation of approximately 1.5 Å for the main chain between the predicted and actual structures [39]. The 3-D structures were optimized thermodynamically by energy minimization using MOE and an AMBER99 force field [44] and further refined the physically unacceptable local structures on the basis of evaluation of unusual dihedral angles, *phi* and *psi*, by the Ramachandran plot using MOE. The binding energies of the CA dimer models, E_{bind}, were calculated as described elsewhere [45,46], using the formula $E_{bind} = E_{dimer} - 2E_{monomer}$, where E_{dimer} is the energy of the CA dimer; $E_{monomer}$ is the energy of the CA monomer.

Conclusions

The CA of HIV-2 CRF01_AB isolates have a unique feature distinct from that of other HIV-2 strains; CRF01_AB-specific sequences conferred strong resistance to human TRIM5α. CRF01_AB-specific amino acid substitutions in the CA CTD were necessary for strong resistance to human TRIM5α.

Supporting Information

Figure S1 Western blot analysis of TRIM5α proteins. HA-tagged TRIM5α proteins in lysate of CEM-SS cells infected with recombinant SeV were visualized by western blotting with an antibody against HA. S(-), Hu, CM, and Rh denote CM SPRY(-), human, cynomolgus monkey, and rhesus TRIM5α, respectively. Molecular weight makers are shown on the left.
(EPS)

Acknowledgments

We thank Dr. Y. Tian, Dr. S. Nakamura and Dr. T. Yasunaga for helpful discussions, and Ms. S. Bando and Ms. N. Teramoto for assistance.

Author Contributions

Conceived and designed the experiments: TM EEN SI HS TS. Performed the experiments: TM EEN MY ST KK. Analyzed the data: TM EEN MY SI KK JL WS HS TS. Contributed reagents/materials/analysis tools: SI YY MP JL WS. Wrote the paper: TM EEN MY SI JL HS TS.

References

1. Rowland-Jones SL, Whittle HC (2007) Out of Africa: what can we learn from HIV-2 about protective immunity to HIV-1? Nat Immunol 8: 329–331.
2. Gao F, Bailes E, Robertson DL, Chen Y, Rodenburg CM, et al. (1999) Origin of HIV-1 in the chimpanzee Pan troglodytes troglodytes. Nature 397: 436–441.
3. Huet T, Cheynier R, Meyerhans A, Roelants G, Wain-Hobson S (1990) Genetic organization of a chimpanzee lentivirus related to HIV-1. Nature 345: 356–359.
4. Gottlieb GS, Sow PS, Hawes SE, Ndoye I, Redman M, et al. (2002) Equal plasma viral loads predict a similar rate of CD4+ T cell decline in human immunodeficiency virus (HIV) type 1- and HIV-2-infected individuals from Senegal, West Africa. J Infect Dis 185: 905–914.
5. Damond F, Worobey M, Campa P, Farfara I, Colin G, et al. (2004) Identification of a highly divergent HIV type 2 and proposal for a change in HIV type 2 classification. AIDS Res Hum Retroviruses 20: 666–672.
6. Stremlau M, Owens CM, Perron MJ, Kiessling M, Autissier P, et al. (2004) The cytoplasmic body component TRIM5alpha restricts HIV-1 infection in Old World monkeys. Nature 427: 848–853.

7. Sebastian S, Luban J (2005) TRIM5alpha selectively binds a restriction-sensitive retroviral capsid. Retrovirology 2: 40.
8. Stremlau M, Perron M, Lee M, Li Y, Song B, et al. (2006) Specific recognition and accelerated uncoating of retroviral capsids by the TRIM5alpha restriction factor. Proceedings of the National Academy of Sciences of the United States of America 103: 5514–5519.
9. Reymond A, Meroni G, Fantozzi A, Merla G, Cairo S, et al. (2001) The tripartite motif family identifies cell compartments. Embo J 20: 2140–2151.
10. Nakayama EE, Miyoshi H, Nagai Y, Shioda T (2005) A specific region of 37 amino acid residues in the SPRY (B30.2) domain of African green monkey TRIM5alpha determines species-specific restriction of simian immunodeficiency virus SIVmac infection. Journal of Virology 79: 8870–8877.
11. Hatziioannou T, Perez-Caballero D, Yang A, Cowan S, Bieniasz PD (2004) Retrovirus resistance factors Refl and Lv1 are species-specific variants of TRIM5alpha. Proceedings of the National Academy of Sciences of the United States of America 101: 10774–10779.
12. Keckesova Z, Ylinen LM, Towers GJ (2004) The human and African green monkey TRIM5alpha genes encode Refl and Lv1 retroviral restriction factor activities. Proceedings of the National Academy of Sciences of the United States of America 101: 10780–10785.
13. Perron MJ, Stremlau M, Song B, Ulm W, Mulligan RC, et al. (2004) TRIM5alpha mediates the postentry block to N-tropic murine leukemia viruses in human cells. Proceedings of the National Academy of Sciences of the United States of America 101: 11827–11832.
14. Nakayama EE, Shioda T (2010) Anti-retroviral activity of TRIM5 alpha. Rev Med Virol 20: 77–92.
15. Song H, Nakayama EE, Yokoyama M, Sato H, Levy JA, et al. (2007) A single amino acid of the human immunodeficiency virus type 2 capsid affects its replication in the presence of cynomolgus monkey and human TRIM5alphas. Journal of Virology 81: 7280–7285.
16. Price AJ, Marzetta F, Lammers M, Ylinen LM, Schaller T, et al. (2009) Active site remodeling switches HIV specificity of antiretroviral TRIMCyp. Nat Struct Mol Biol 16: 1036–1042.
17. Gamble TR, Yoo S, Vajdos FF, von Schwedler UK, Worthylake DK, et al. (1997) Structure of the carboxyl-terminal dimerization domain of the HIV-1 capsid protein. Science 278: 849–853.
18. Onyango CO, Leligdowicz A, Yokoyama M, Sato H, Song H, et al. (2010) HIV-2 capsids distinguish high and low virus load patients in a West African community cohort. Vaccine 28S2: B60–B67.
19. Ibe S, Yokomaku Y, Shiino T, Tanaka R, Hattori J, et al. (2010) HIV-2 CRF01_AB: first circulating recombinant form of HIV-2. J Acquir Immune Defic Syndr 54: 241–247.
20. Marlink R, Kanki P, Thior I, Travers K, Eisen G, et al. (1994) Reduced rate of disease development after HIV-2 infection as compared to HIV-1. Science 265: 1587–1590.
21. Miyamoto T, Yokoyama M, Kono K, Shioda T, Sato H, et al. (2011) A single amino acid of human immunodeficiency virus type 2 capsid protein affects conformation of two external loops and viral sensitivity to TRIM5alpha. PloS one 6: e22779.
22. Kono K, Song H, Shingai Y, Shioda T, Nakayama EE (2008) Comparison of anti-viral activity of rhesus monkey and cynomolgus monkey TRIM5alphas against human immunodeficiency virus type 2 infection. Virology 373: 447–456.
23. Wu X, Anderson JL, Campbell EM, Joseph AM, Hope TJ (2006) Proteasome inhibitors uncouple rhesus TRIM5alpha restriction of HIV-1 reverse transcription and infection. Proceedings of the National Academy of Sciences of the United States of America 103: 7465–7470.
24. Anderson JL, Campbell EM, Wu X, Vandegraaff N, Engelman A, et al. (2006) Proteasome inhibition reveals that a functional preintegration complex intermediate can be generated during restriction by diverse TRIM5 proteins. Journal of Virology 80: 9754–9760.
25. Pertel T, Reinhard C, Luban J (2011) Vpx rescues HIV-1 transduction of dendritic cells from the antiviral state established by type 1 interferon. Retrovirology 8: 49.
26. Sokolskaja E, Berthoux L, Luban J (2006) Cyclophilin A and TRIM5alpha independently regulate human immunodeficiency virus type 1 infectivity in human cells. Journal of Virology 80: 2855–2862.
27. Pertel T, Hausmann S, Morger D, Zuger S, Guerra J, et al. (2011) TRIM5 is an innate immune sensor for the retrovirus capsid lattice. Nature 472: 361–365.
28. Kono K, Song H, Yokoyama M, Sato H, Shioda T, et al. (2010) Multiple sites in the N-terminal half of simian immunodeficiency virus capsid protein contribute to evasion from rhesus monkey TRIM5alpha-mediated restriction. Retrovirology 7: 72.
29. Pornillos O, Ganser-Pornillos BK, Kelly BN, Hua Y, Whitby FG, et al. (2009) X-ray structures of the hexameric building block of the HIV capsid. Cell 137: 1282–1292.
30. Ganser-Pornillos BK, Yeager M, Sundquist WI (2008) The structural biology of HIV assembly. Curr Opin Struct Biol 18: 203–217.
31. Inagaki N, Takeuchi H, Yokoyama M, Sato H, Ryo A, et al. (2010) A structural constraint for functional interaction between N-terminal and C-terminal domains in simian immunodeficiency virus capsid proteins. Retrovirology 7: 90.
32. Bailey GD, Hyun JK, Mitra AK, Kingston RL (2012) A structural model for the generation of continuous curvature on the surface of a retroviral capsid. J Mol Biol 417: 212–223.
33. Gao F, Yue L, White AT, Pappas PG, Barchue J, et al. (1992) Human infection by genetically diverse SIVSM-related HIV-2 in west Africa. Nature 358: 495–499.
34. Hillis DM, Bull JJ (1993) An empirical test of bootstrapping as a method for assessing confidence in phylogenetic analysis. Syst Biol 42: 182–192.
35. Pear WS, Nolan GP, Scott ML, Baltimore D (1993) Production of high-titer helper-free retroviruses by transient transfection. Proc Natl Acad Sci U S A 90: 8392–8396.
36. Lasfargues EY, Lasfargues JC, Dion AS, Greene AE, Moore DH (1976) Experimental infection of a cat kidney cell line with the mouse mammary tumor virus. Cancer Res 36: 67–72.
37. Sheehy AM, Gaddis NC, Choi JD, Malim MH (2002) Isolation of a human gene that inhibits HIV-1 infection and is suppressed by the viral Vif protein. Nature 418: 646–650.
38. Dodson GG, Lane DP, Verma CS (2008) Molecular simulations of protein dynamics: new windows on mechanisms in biology. EMBO Rep 9: 144–150.
39. Baker D, Sali A (2001) Protein structure prediction and structural genomics. Science 294: 93–96.
40. Shirakawa K, Takaori-Kondo A, Yokoyama M, Izumi T, Matsui M, et al. (2008) Phosphorylation of APOBEC3G by protein kinase A regulates its interaction with HIV-1 Vif. Nat Struct Mol Biol 15: 1184–1191.
41. Case DA, Darden TA, Cheatham I, T.E., Simmerling CL, Wang JR, et al. (2006) AMBER 9. University of California, San Francisco.
42. Hornak V, Abel R, Okur A, Strockbine B, Roitberg A, et al. (2006) Comparison of multiple Amber force fields and development of improved protein backbone parameters. Proteins 65: 712–725.
43. Ryckaert J-P, Ciccotti G, Berendsen HJC (1977) Numerical integration of the cartesian equations of motion of a system with constraints: Molecular dynamics of n-alkanes. J Comput Phys 23: 327–341.
44. Ponder JW, Case DA (2003) Force fields for protein simulations. Adv Protein Chem 66: 27–85.
45. Lee K, Chu CK (2001) Molecular modeling approach to understanding the mode of action of L-nucleosides as antiviral agents. Antimicrob Agents Chemother 45: 138–144.
46. Kinomoto M, Yokoyama M, Sato H, Kojima A, Kurata T, et al. (2005) Amino acid 36 in the human immunodeficiency virus type 1 gp41 ectodomain controls fusogenic activity: implications for the molecular mechanism of viral escape from a fusion inhibitor. Journal of Virology 79: 5996–6004.

Cell Host & Microbe
Article

Antimicrobial Peptide LL-37 Produced by HSV-2-Infected Keratinocytes Enhances HIV Infection of Langerhans Cells

Youichi Ogawa,[1] Tatsuyoshi Kawamura,[1,*] Takamitsu Matsuzawa,[1] Rui Aoki,[1] Peter Gee,[4] Atsuya Yamashita,[2] Kohji Moriishi,[2] Kenshi Yamasaki,[3] Yoshio Koyanagi,[4] Andrew Blauvelt,[5] and Shinji Shimada[1]
[1]Department of Dermatology
[2]Department of Microbiology
Faculty of Medicine, University of Yamanashi, Yamanashi 409-3898, Japan
[3]Department of Dermatology, Tohoku University Graduate School of Medicine, Sendai 980-8575, Japan
[4]Laboratory of Viral Pathogenesis, Institute for Virus Research, Kyoto University, Kyoto 606-8507, Japan
[5]Oregon Medical Research Center, Portland, OR 97223, USA
*Correspondence: tkawa@yamanashi.ac.jp
http://dx.doi.org/10.1016/j.chom.2012.12.002

SUMMARY

Herpes simplex virus (HSV)-2 shedding is associated with increased risk for sexually acquiring HIV. Because Langerhans cells (LCs), the mucosal epithelium resident dendritic cells, are suspected to be one of the initial target cell types infected by HIV following sexual exposure, we examined whether and how HSV-2 affects HIV infection of LCs. Although relatively few HSV-2/HIV-coinfected LCs were detected, HSV-2 dramatically enhanced the HIV susceptibility of LCs within skin explants. HSV-2 stimulated epithelial cell production of antimicrobial peptides (AMPs), including human β defensins and LL-37. LL-37 strongly upregulated the expression of HIV receptors in monocyte-derived LCs (mLCs), thereby enhancing their HIV susceptibility. Culture supernatants of epithelial cells infected with HSV-2 enhanced HIV susceptibility in mLCs, and this effect was abrogated by blocking LL-37 production. These data suggest that HSV-2 enhances sexual transmission of HIV by increasing HIV susceptibility of LCs via epithelial cell production of LL-37.

INTRODUCTION

Epidemiologic studies have indicated a strong association between the acquisition of HIV and other sexually transmitted diseases (STDs) (Galvin and Cohen, 2004). This link is especially evident in cases of genital ulcer diseases (GUDs), with a 2- to 11-fold increase in the rate of HIV acquisition in the presence of GUD (Cameron et al., 1989; Fleming and Wasserheit, 1999). It is widely recognized that herpes simplex virus type 2 (HSV-2) is a major cause of GUDs, and more than 50 epidemiologic studies have now indicated that HSV-2 shedding is associated with increased risk for acquiring HIV (Wald and Link, 2002). The risk ratio of HIV acquisition for a person with genital herpes is enhanced from 2 to 4 when compared with a person without genital herpes, and potentially 50% of new HIV infections are considered to be attributable or worsened by HSV-2 infection (Wald and Link, 2002).

During sexual transmission of HIV, virus crosses mucosal epithelium and is eventually transmitted to regional lymph nodes, where it establishes permanent infection. Many studies have shown that Langerhans cells (LCs) are one of the important initial cellular targets for HIV, and that this particular type of dendritic cell (DC) plays a crucial role in disseminating HIV (de Witte et al., 2007; Kawamura et al., 2005; Lederman et al., 2006; Shattock and Moore, 2003). LCs are present within genital skin (e.g., outer foreskin) and mucosal epithelium and, after contact with pathogens, readily emigrate from tissue to draining lymph nodes. Immature resident LCs express surface CD4 and CCR5, but not surface CXCR4 (Zaitseva et al., 1997). These LCs are readily infected ex vivo with R5 HIV, but not with X4 HIV (Kawamura et al., 2000, 2008; Reece et al., 1998; Zaitseva et al., 1997). These findings are consistent with previous epidemiologic observations, which have found that the majority of HIV strains isolated from newly infected patients are R5 HIV strains (Zhu et al., 1993). It has been reported that persons with *CCR5* homozygous defects are largely protected from sexually acquiring HIV (Liu et al., 1996).

Clinical trials performed over the last several years have shown that circumcision greatly reduces the probability of penile HIV transmission, suggesting that the foreskin is an important portal of HIV entry (Auvert et al., 2005; Bailey et al., 2007; Gray et al., 2007). Although the mechanism leading to protection remains undefined, several ex vivo experiments with foreskin explants have indicated that CD4 T lymphocytes and LCs within foreskin epidermis are initial target cells for HIV (Fahrbach et al., 2010; Ganor et al., 2010; Grivel et al., 2011; Zhou et al., 2011).

In primate models of simian immunodeficiency virus (SIV) infection, there is controversy regarding which cells in the genital mucosa are initially infected by SIV. Studies have demonstrated that the primary infected cells present in the lamina propria of the cervicovaginal mucosa 48–72 hr after intravaginal exposure to SIV are T cells or submucosal DCs, but not epithelial LCs (Spira et al., 1996; Zhang et al., 1999). When vaginal tissue was examined within 1 hr following vaginal inoculation, however, up to

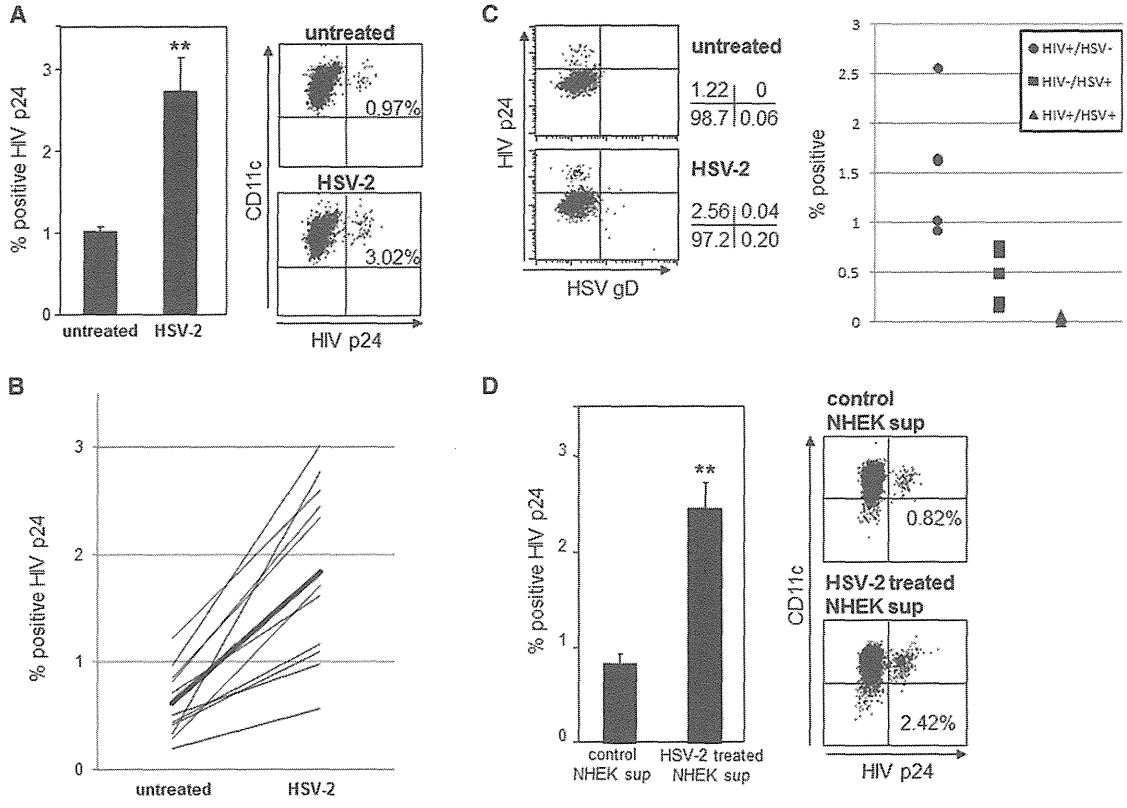

Figure 1. HSV-2-Infected Epithelial Cells Augment HIV Infection in LCs

(A–C) Epithelial sheets were preincubated with HSV-2 and then exposed to R5 HIV. Epithelial sheets were floated on culture medium to allow migration of LCs from the explants. Emigrating cells from the epidermal sheets were collected 3 days following HIV exposure. HIV-infected LCs were assessed by HIV p24 intracellular staining in langerin$^+$ CD11c$^+$ LCs (A) and the results of 11 separate experiments with different donors are summarized (B). HSV− and/or HIV-infected LCs were assessed by HIV p24 and HSV gD intracellular staining in CD11c$^+$ LCs, and the results from five different donors are summarized (C).

(D) mLCs were preincubated with the supernatants from NHEKs treated with or without HSV-2, and then exposed to R5 HIV. HIV p24$^+$ cells were assessed in langerin$^+$ CD11c$^+$ mLCs at day 7.

(A, C, and D) Representative flow cytometric analyses are shown. (A and D) Results are shown as means ± SD (n = 3) (**$p < 0.01$). See also Figure S1.

90% of SIV-infected cells were found to be LCs (Hu et al., 2000). Because only a single layer of columnar epithelium guards the endocervix and the transformation zone, the mucosal barrier can be easily breached by mechanisms such as the microtrauma associated with sexual intercourse, which provides immediate access to target cells, especially CD4$^+$ T cells, in the submucosa (Haase, 2010). Indeed, it has been shown that following mucosal exposure to high doses of SIV, virus can gain access through breaks in the mucosal epithelial barrier and infect resting CD4$^+$ T cells in the submucosa (Haase, 2010). Since molecules targeting CCR5 completely protected against mucosal transmission of SHIV (Lederman et al., 2004), CD4/CCR5-mediated de novo infection of LCs and/or CD4$^+$ T cells is considered to be a major pathway involved in sexual transmission of HIV.

Several mechanisms have been proposed to explain enhanced sexual transmission of HIV during active STD infection, including breakdown of epithelial barriers (i.e., ulceration) with direct inoculation of HIV into the blood (Cunningham et al., 1985), presence of inflammatory leukocytes that act as targets (Zhu et al., 2009), and coinfection of cells by HIV and STD pathogens. Biological mechanisms responsible for greater HIV transmission rates in the presence of genital herpes infections, however, are as of yet unknown. Recently, we and others have suggested that HIV susceptibility of LCs could be directly enhanced by pathogens and indirectly enhanced by inflammatory factors during STD, thereby leading to more likely sexual transmission of HIV (de Jong et al., 2008; Ogawa et al., 2009). In this report, we found that HSV-2 primarily infected epithelial cells and then markedly enhanced HIV infection in adjacent LCs. Interestingly, mechanistic studies revealed that LL-37 produced by HSV-2-infected epithelial cells upregulated CD4 and CCR5 on the surface of bystander LCs, thereby enhancing HIV infection in these cells. These findings may lead to new strategies designed to block sexual transmission of HIV.

RESULTS

HSV-2 Indirectly Enhances HIV Susceptibility in LCs via Interaction with Epithelial Cells

We first examined whether HSV-2 modulates HIV susceptibility of LCs by using an ex vivo skin explant model, whereby resident LCs within epithelial tissue are exposed to HIV and then allowed to emigrate from tissue, thus mimicking conditions that occur following mucosal exposure to HIV (Kawamura et al., 2000).

LL-37 Enhances HIV Infection of Langerhans Cells

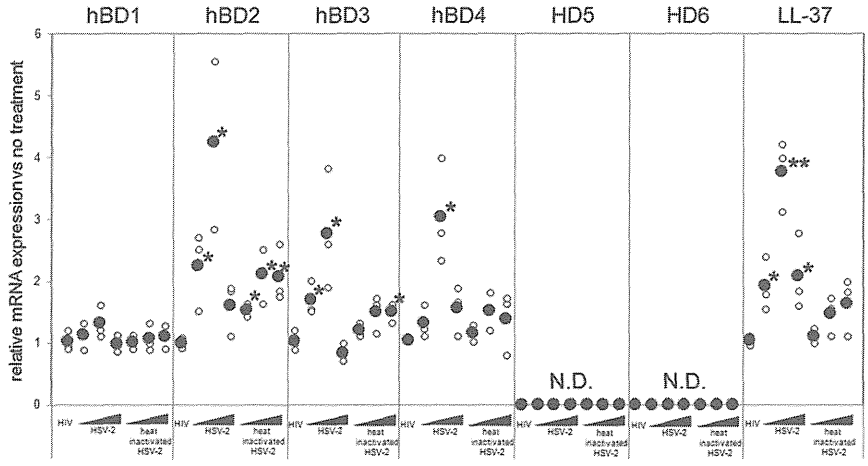

Figure 2. HSV-2 Increases Expression of Human β Defensin-2, Defensin-3, Defensin-4, and LL-37 in Normal Human Epithelial Cells

HIV-1 (10^5 $TCID_{50}$), HSV-2 ($1 \times 10^4 - 1 \times 10^6$ PFU), and heat-inactivated HSV-2 ($1 \times 10^4 - 1 \times 10^6$ PFU) were exposed to NHEKs for 1 hr and then washed twice. Cells were incubated in culture medium for 12 hr, and the mRNA expression of indicated AMPs was determined by qPCR. Results are shown as mean relative mRNA expressions (○) from three different experiments and mean the average (●) of those (*$p < 0.05$; **$p < 0.01$). See also Figure S2.

Epidermal sheets obtained from suction blister roofs were exposed to HSV-2 strain G at 1×10^6 PFU/tissue for 1 hr, and then exposed to R5-tropic HIV-1_{BaL} for 2 hr. Three days later, to quantify numbers of HIV-infected LCs at the single-cell level, cells emigrating from the explants were stained with anti-CD11c, anti-langerin, and anti-HIV p24 mAbs. Intracellular staining for HIV p24 represents productive HIV replication within LCs, since expression can be completely blocked by AZT (Kawamura et al., 2003). The numbers of LCs emigrating from individual explants were determined, and the mean yield ± SD was HSV−/HIV−; 1.04 ± 0.25 × 10^4, HSV−/HIV+; 1.13 ± 0.31 × 10^4, HSV+/HIV−; 1.25 ± 0.27 × 10^4; and HSV+/HIV+; 1.21 ± 0.25 × 10^4 (n = 3). Thus, the number of LCs recovered from the skin explants was not significantly affected by HSV-2 or HIV exposure. However, preincubation of epithelial sheets with HSV-2 significantly increased the percentage of HIV $p24^+$ cells within $langerin^+$ $CD11c^+$ LCs approximately 3-fold as compared to LCs emigrating from nonexposed epithelial sheets (Figure 1A). The results of 11 separate experiments with different skin donors are summarized in Figure 1 B (mean percentage HIV $p24^+$ LCs ± SD = 0.61 ± 0.31 with no HSV-2; 1.85 ± 0.79 with HSV-2 preincubation, p = 0.0002, n = 11). To assess the ratio of individual HSV-2- and/or HIV-infected LCs emigrating from explants, cells were collected from cultures and stained with anti-CD11c, anti-HSV gD, and anti-HIV p24 mAbs. A recent study in mice showed that HSV impeded emigration of infected LCs by inducing apoptosis and by blocking E-cadherin downregulation (Miller et al., 2011b). Consistent with this finding, the percentage of HSV-2-infected emigrating LCs was much less when compared with LCs that remained within explants at day 3 (Figure 1C and see Figure S1 online). More importantly, we found that HSV-2/HIV-coinfected emigrating LCs were rarely detected (mean percentage of HIV-1 $p24^+$/HSV-2 gD^+ LCs ± SD = 0.04 ± 0.02, n = 5, Figure 1C), suggesting that HSV may not directly modulate HIV susceptibility in LCs. Indeed, supernatants from epithelial cell cultures of normal human epidermal keratinocytes (NHEKs) treated with HSV-2 also increased the percentage of HIV p24+ monocyte-derived LCs (mLCs), even though mLCs were not exposed to HSV-2 (Figure 1D). Of note, the magnitude of HIV susceptibility in mLCs enhanced by HSV-treated NHEK supernatants was comparable to that in emigrating LCs in the epithelial explant experiments. Enhancement of HIV infection by supernatants from HSV-2-treated NHEKs was dependent on the dose of HSV-2, and supernatants from heat-inactivated HSV-2-treated NHEKs did not affect HIV susceptibility in mLCs (Figure S2). HIV susceptibility in mLCs was also enhanced when we infected NHEKs with a second HSV-2 strain, 186 (data not shown). Taken together, these results suggest that HSV-2 indirectly mediates HIV infection of epidermal LCs by a soluble factor or factors released by HSV-2-infected epithelial cells.

HSV-2 Augments the Production of Antimicrobial Peptides from Keratinocytes, and LL-37 Enhances HIV Infection in LCs

In STDs, antimicrobial peptides (AMPs), including defensins and cathelicidin, are the key effector molecules of mucosal innate and adaptive immunity. Human vaginal epithelial cells and epidermal keratinocytes can produce human α defensin-5 (HD5), HD6 and human β defensin-1 (hBD1), hBD2, hBD3, hBD4, and the sole cathelicidin in humans, LL-37. Certain defensins (e.g., hBD1) are expressed constitutively, and others (e.g., hBD2 and hBD3) show increased expression in response to inflammation or infection (Klotman and Chang, 2006). Several reports have indicated that several of these AMPs modulate HIV infectivity in peripheral blood mononuclear cells (PBMC) or in $CD4^+$ T cells (Bergman et al., 2007; Klotman et al., 2008; Quiñones-Mateu et al., 2003; Sun et al., 2005). Thus, we investigated whether HSV-2 induced AMPs production in keratinocytes. NHEKs were incubated with HSV-2 ($1 \times 10^4 - 1 \times 10^6$ PFU) or HIV-1 (1×10^5 $TCID_{50}$), and relative mRNA expression levels of AMPs were determined by quantitative RT-PCR. Interestingly, HSV-2 significantly increased the expression of hBD2, hBD3, hBD4, and LL-37, whereas neither HIV nor heat-inactivated HSV-2 affected expression of hBD3, hBD4, and LL-37 (Figure 2).

To determine whether keratinocyte-derived AMPs affect HIV susceptibility of LCs, mLCs were stimulated with AMPs or TNF-α, as a positive control, for 24 hr before exposure to HIV-1. Strikingly, only LL-37 significantly increased the percentage of HIV $p24^+$ mLCs (Figure 3A). This infection-enhancing effect of LL-37 was observed in a dose-dependent manner, utilizing concentrations of LL-37 observed in physiologic conditions (Ong et al., 2002; Yamasaki et al., 2007) (Figure 3B). Interestingly, LL-37 also significantly upregulated surface expression